Journal of Hydrology: Regional Studies 66 (2026) 103607

Contents lists available at ScienceDirect

Journal of Hydrology: Regional Studies

journal homepage: www.elsevier.com/locate/ejrh

Seawater-freshwater interface dynamics driven by upstream freshwater discharge and tidal oscillations in highly stratified River Neretva estuary

Iva Aljinović [a,*], Veljko Srzić [b], Marin Milin [c]

[a] *Science and Arts Research Logical Unit for Hydrotechnical Engineering, Faculty of Civil Engineering, Architecture and Geodesy, University of Split, Matice Hrvatske 15, Split 21000, Croatia*
[b] *Department of Water Resources, Faculty of Civil Engineering, Architecture and Geodesy, University of Split, Matice Hrvatske 15, Split 21000, Croatia*
[c] *Higra LTD, Doverska 13, Split 21000, Croatia*

A R T I C L E I N F O

Keywords:
River Neretva
Microtidal estuary
Backwater
Salt wedge
Temperature monitoring
Seawater-freshwater interface

A B S T R A C T

Study region: River Neretva estuary, Republic of Croatia
Study focus: The study is focused on understanding of the seawater-freshwater interface (SFI) dynamics driven simultaneously by upstream freshwater discharge (Q_F) and tidal oscillations (h_{SL}) along the dry hydrological period. Implementation of the novel, site specific, water column temperature based monitoring system, in combination with extensive hydrological monitoring, ensures comprehensive and relevant data sets along the 11-day period. Obtained time series are used to reveal frequency similarities and to establish functional dependencies between SFI depth (h_{SFI}) and its driving forces, Q_F and h_{SL}.
New hydrological insights for the region: Water column temperature profiling delineated upper freshwater layer from the bottom seawater layer, thus enabling the determination of the h_{SFI} and correction of Q_F in highly stratified conditions. Novel Q_F offers a superior first order data based framework compared to present discharge assessment. Amplitude spectral density identified matching in frequency constituents, which led to functional interdependence of h_{SFI} to Q_F and h_{SL} in trend and residual components. Linear regression model has been used to establish functional relationship between h_{SFI} and its controlling mechanisms valid during dry season. SFI dynamics are simultaneously controlled by Q_F and h_{SL}, operating on different timescales. While Q_F controls the overall h_{SFI} trend feature, h_{SFI} fluctuations at timescales smaller than daily have been identified to be in correspondence to diurnal and semidiurnal tidal components.

1. Introduction

Estuaries present dynamic environments under complex influence of river freshwater inflow and seawater intrusion (SWI) (Savenije, 2005). These ecosystems form a balance between ecological and socio-economical services (Elliott and Whitfield, 2011) including water supply, domestic and industrial needs, agricultural irrigation, navigation and recreation under constant pressure of preserving its unique biodiversity. A wide range of human impacts compromise sustainability hereby, inducing long-term

* Corresponding author.
E-mail addresses: iva.matic@gradst.hr (I. Aljinović), veljko.srzic@gradst.hr (V. Srzić), higra.ured@gmail.com (M. Milin).

https://doi.org/10.1016/j.ejrh.2026.103607
Received 13 February 2026; Received in revised form 30 May 2026; Accepted 1 June 2026
Available online 4 June 2026

environmental problems (Kennish, 2002). Natural SWI process of in estuaries, when exacerbated by anthropological factors, leads to deterioration of water quality (Werner et al., 2013), absence of suitable freshwater quantity, soil salinization (Mazhar et al., 2022) and riparian saltwater intrusion (Setiawan et al., 2023). Salinity dynamics along the estuaries worldwide have great impact to circulation patterns, water column stratification, mixing, and sediment dynamics (Pritchard, 1955).

The balance between freshwater discharge and tidal mixing determines estuarine mixing regime (Zhang and Savenije, 2018). While the dominance of tidal mixing over freshwater discharge leads to homogeneous salinity distribution along the water column (MacCready and Geyer, 2010), prevalence of freshwater discharge over tidal mixing results in a strongly stratified two-layer flow where a sharp seawater freshwater interface (SFI) separates the overlying freshwater from the underlying seawater, a structure commonly referred to as a salt wedge (Geyer and Ralston, 2011) which represents the boundary extreme of highly stratified conditions as found in estuaries.

In microtidal estuaries, the presence of salt wedge and stratified flow occurs under low freshwater discharge from the upstream, since forcing from river discharge typically dominates over weak tidal forcing thus mixing between freshwater and seawater layer diminishes (Geyer and MacCready, 2014).

Literature review highlights freshwater discharge and seawater level as factors dominantly controlling SWI intensity in estuaries (He et al., 2018), with tidal oscillations (Khojasteh et al., 2021), river channel geometry (Nguyen et al., 2012), extreme meteorological events (Perales-Valdivia et al., 2018), wind generated waves (Higgins Álvarez et al., 2022), combination of storm events and waves (Postacchini et al., 2023) and anthropogenic activities (Li et al., 2020) contributing the SWI phenomena in estuaries over characteristic time scales. By quantifying the influence of freshwater discharge on salt wedge position, (Geyer and Ralston, 2011) expression derived from a two-layer hydraulic theory has been developed in a form $L \sim Q^{-n}$. This theory has been used at different sites as initial assessment of salt wedge intrusion length by adapting the exponent value n in accordance to locally found peculiarities (Poggioli and Horner-Devine, 2015).

The role of tidal oscillations is enhanced mostly when seasonal variability of SWI in estuaries is of interest (Cardona et al., 2025). During dry periods characterised by lower freshwater discharge occurrence, tidal forcing controls the upstream salt wedge intrusion, whereas intrusion is substantially restricted during periods of high freshwater discharge (Kostaschuk and Atwood, 1990; Cordero-Acosta et al., 2024). Seasonal variability of combined influence of freshwater discharge and tidal oscillations to river salinity has been analysed in the study of Magdalena River estuary (Otero et al., 2021) by MOHID implementation. Similar study has been conducted at Volturno River using combined HEC-RAS and spectral analysis approach (Gaiolini et al., 2023). In both studies tidal action mainly caused minor daily variations in the salt wedge's horizontal position (up to 1 km), but did not alter the stratified nature of the system, emphasizing the dominance of freshwater discharge hereby.

While the influence of controlling factors to salt wedge length has been extensively studied up to date, combined effects of these factors to the SFI depth remain of less interest. (McKeon et al., 2021) investigated the influence of flood and ebb tide on the interface height, with focus to the low-pass filtered 21 psu isohaline. Results indicate that the interface height during the flood phase is largely insensitive to variations in river discharge, whereas the ebb phase exhibits a pronounced dependence on discharge conditions. Although the salt wedge length and volume have been of primary interest within the research community up to date, setting up boundary conditions for assessing the salinization of the coastal aquifers from the river is dominantly controlled by the salt wedge height controlling the inflow surface, highlighting the necessity to improve the knowledge on the salt wedge height transient features.

Freshwater discharge dominance in controlling SWI in microtidal estuaries emphasize the need for its precise determination since relatively small variations in discharge values can induce significant shifts in the salt wedge length and SFI depth (Geyer and Ralston, 2011). While the assessment of river discharge from continuous stream velocity measurements with an acoustic Doppler current profiler (H-ADCP) is one of the most common used methods, accurate freshwater discharge in highly stratified estuaries presents challenging task (Hidayat et al., 2011). The seaward flow of river discharge within a surface layer, combined with the landward SWI along the bottom layer, require observation setup capable to capture stream velocities at multilevel depth. Although single-transect ADCP is able to reveal an estuarine circulation pattern of outflow in the surface layer and inflow in the bottom layer for one cross-section (Reed et al., 2004), the complexity of data acquisition and processing limits its applicability for real-time monitoring compared to surface water elevation observations. While discharge determination in not tidal dominated rivers relies dominantly on the surface water elevation estimation, tidal driven river poses a challenge. In tidal rivers, surface water level is partially controlled by both tidal mechanisms and river discharge (Hidayat et al., 2014) thus highlighting the obstacles in establishing unique functional relationships between surface water elevation and discharge (Lee et al., 2021).

Most common monitoring procedures to define SFI transient nature include electrical conductivity (EC) and temperature (T) measurement at specific depth of water column (CTD profiling). Major obstacle to establish continuous real time SFI monitoring is evidenced in the high cost of commercial equipment, most usually used EC probes and high demanding and frequent on-site maintenance and calibration particularly related to the use of EC sensors (Chong et al., 2014). While advanced techniques for monitoring and predicting the SWI, including UAV and satellite-based imagery combined with machine-learning approaches (Jiang et al., 2024) and data-driven models such as Long Short-Term Memory (LSTM) networks (Rummel et al., 2025; Wullems et al., 2023) demonstrated significant progress in the development of monitoring frameworks and forecasting capabilities, remains a necessity for simpler, cost-effective, and easily transferable methods that can be reliably implemented in data-limited and resource-constrained estuarine environments.

River Neretva and its coastal aquifer has been subject of several studies analysing SWI. Initial numerical modelling of stratified flow in the River Neretva, considering a riverine discharge and seawater level as main SWI controlling mechanisms, indicated the presence of SWI at Metković bridge profile, 25 km inland from the river mouth for discharge values lower than 180 $m^3\ s^{-1}$ and its complete diminishing for discharge values above 500 $m^3\ s^{-1}$(Ljubenkov and Vranješ, 2012). Salt-wedge quasi stationary features were investigated based on monitoring obtained data and two-layer shallow-water numerical model in the period 2015–2018 in (Krvavica et al., 2021) whose results confirmed the presence of salt wedge more than 20 km upstream from the mouth during the dry period of the year. In similar manner, by application of 1D two layer model the impact of mean sea level rise in microtidal salt-wedge estuaries was investigated in the River Neretva estuary (Krvavica and Ružić, 2020). Results indicated sea level rise may increase salt-wedge intrusion length, volume and river stream flow, emphasizing climate change influence importance. River Neretva has been identified as a dominant source of SWI into unconfined aquifer compared to the Adriatic Sea (Lovrinović et al., 2021) during dry season (May-October), mostly by riparian saltwater intrusion, thus enhancing the importance of the knowledge of salt wedge transience along the Neretva estuary.

Due to its substantial hydropower potential, with several hydropower plants (HPP's) constructed along the Neretva River and its basin, the discharge is regulated and significantly altered compared to its natural regime. Although the discharge regulation

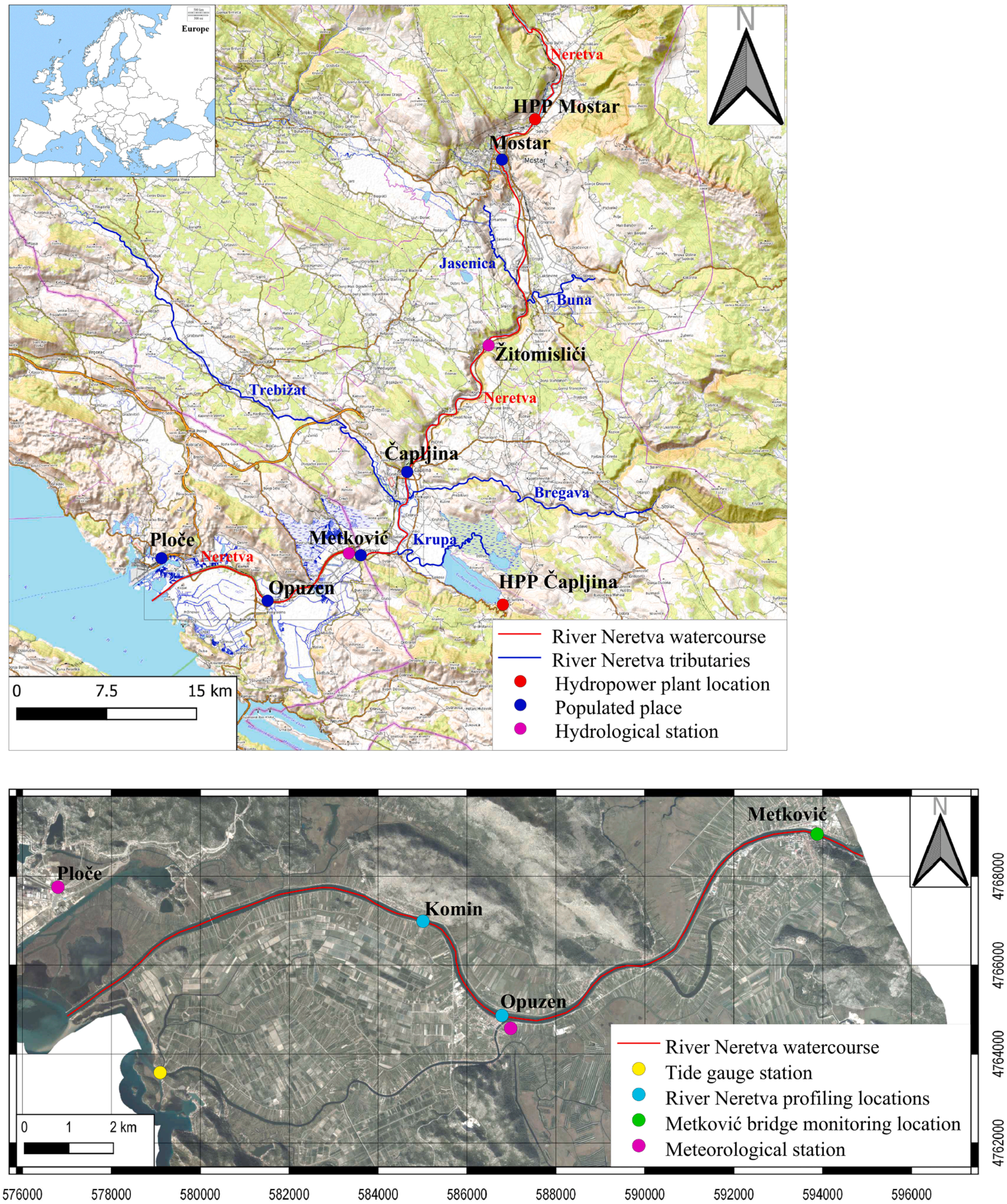

Fig. 1. River Neretva catchment with major tributaries (top) and monitoring locations from the Adriatic Sea to the Metković bridge profile (bottom).

contributes to flood prevention downstream during rain season, it disables freshwater discharge greater than the biological minimum to confront and retreat the salt wedge downstream during dry season. Hydrological station Metković bridge located 20.9 km upstream from the river mouth enables the insight to River Neretva discharge values. Although dislocated from the river mouth upstream, it has been evidenced the complexity of the observed discharge values interpretation hereby stems from two sources. Initially, the presence of significant water column stratification during low discharge occurrence delineates the total flux into two components: upstream seawater flux characterising the bottom layer and downstream freshwater flux characterizing surface layer. Furthermore, tidal propagation effects have been evidenced to influence the discharge values. Both mechanisms are present during dry hydrological periods when discharge values are found below approximately 300 $m^3 s^{-1}$ (FGAG, 2023).

Within the manuscript, we highlight several contributing issues relying on the monitoring capacity to assess the SFI depth in tidal dominated estuary of the Neretva river which enables determination of its dynamic nature when influenced by combined effects of freshwater discharge upstream and Adriatic Sea tidal induced surface elevation downstream.

Main contributions of the manuscript include the development and implementation of a novel temperature based real time monitoring system in the Neretva estuary, followed by the sea and river surface elevation and stream velocity monitoring. Furthermore, the paper introduces framework for the upstream freshwater discharge assessment during the dry hydrological period in tidally dominated estuary backwater zone, and finally, the study provides insight to the combined effects of freshwater discharge and seawater level as main driving forces controlling the SFI depth dynamics in River Neretva estuary.

To our best knowledge, this paper offers novel insights to Neretva estuary conditions and applicative monitoring solutions with emphasis to SFI dynamic features determination. Even though the SWI intrusion length in the River Neretva has been a subject of research in the past (Krvavica et al., 2021), up to date no significant contribution in the SFI depth forcing has been reported.

2. Methodology and site application

To achieve goals identified within the Introduction section, a methodical approach has been set up as follows: i) design, implementation and putting into operation of novel monitoring infrastructure at Metković bridge hydrological station, ii) development of the framework to determine the upstream freshwater discharge in highly stratified estuaries and iii) analysis to perform the SFI dynamics when controlled by upstream freshwater discharge and tides simultaneously.

2.1. Study area

River Neretva is the longest karstic river in the Eastern Adriatic passing through Bosnia and Herzegovina (205 km) and Croatia (last 21.7 km) before reaching the Adriatic Sea through the delta (Fig. 1). Its natural hydrological pattern has been changed significantly from 1960's when first melioration activities have been implemented in the area followed by the upstream HPP induced regulation. Combined effects of both hydropower infrastructure and melioration regulation lead to the decrease of the water level beneath the ground level thus separating the estuary from the delta and transforming the delta into greatest agricultural area along the Adriatic east coast (Srzić et al., 2020; Lovrinović et al., 2023; Racetin et al., 2020).

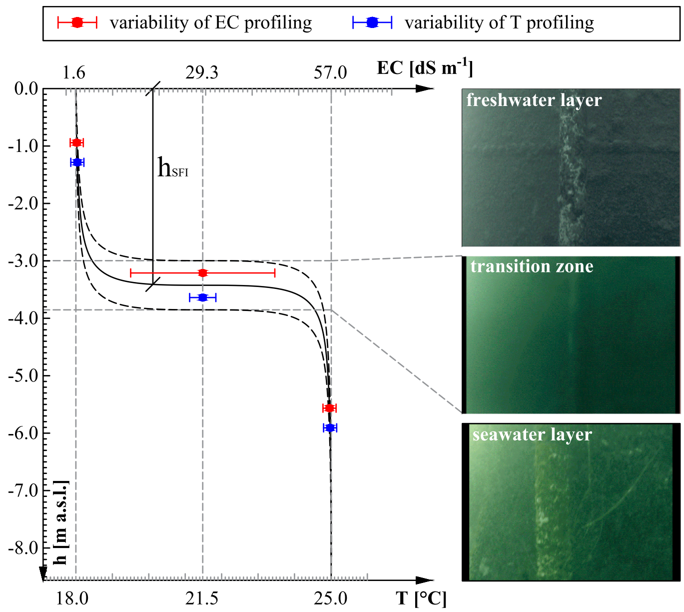

Fig. 2. Vertical stratification of the water column EC and T with box-plot variability of EC and T profiles (left), and underwater photographs from the Metković bridge site (right) obtained during the profiling on September 5th 2024.

Present river Neretva's lower course forms a microtidal estuary (Savenije, 2005), characterized by tidal amplitude typically less than 0.3 m (Janeković and Kuzmić, 2005) with an interaction of upstream river discharge and Adriatic Sea surface elevation controlling complex seawater intrusion mechanisms along the estuary (FGAG, 2023), (Lovrinović et al., 2023).

Hydrological character reveals seasonal fluctuations driven by the amount of precipitation over the river basin during rain period and the operational regime of the Mostar HPP, located 40 km upstream in Bosnia and Herzegovina, during dry period. Mean annual precipitation for the period 2009–2024, derived from continuous measurements at the Ploče and Opuzen meteorological stations, amounts to 1146 mm year^{-1} and 1200 mm year^{-1} , respectively.

For the corresponding time span, observed discharge varied between 40 m^3 s^{-1} and 2092 m^3 s^{-1} while the long-term (2009–2024) mean annual discharge equals 340 m^3 s^{-1}. The amount of 40 m^3 s^{-1} represents the biological minimum released from the upstream Mostar HPP. Dry season (from May to October) fluctuations are found within the range between 40 m^3 s^{-1} and 250 m^3 s^{-1} with occasional peaks above 250 m^3 s^{-1}, unless discharge values between 250 m^3 s^{-1} and 1700 m^3 s^{-1} usually characterise on average rain season (from November to April).

The Adriatic Sea tidal regime is characterized by mixed diurnal–semidiurnal pattern, with pronounced differences in tidal amplitudes between neap and spring tides (Janeković and Kuzmić, 2005). In Srzić et al. (2020) four predominant tidal constituents in sea level data were identified for the period of August 2015, including diurnal components O1 and K1 and M2 and S2 as semidiurnal ones.

2.2. Temperature-based seawater-freshwater interface dynamics monitoring

To overcome peculiarities related to traditional use of EC sensors reported within the Introduction section as well as to ensure potentially reliable, low level uncertainty, real time insight to water column stratification in salt wedge estuaries, the alternative has been recognised in the T based monitoring (Fig. 2).

To demonstrate superiority of the T over the EC in practical application, a series of continuous water column profiling has been performed at river Neretva Metković bridge profile (Fig. 1) by using SEBA KLL-Q−2 multiparameter probe. Profiling has been performed during dry conditions fulfilling the pre assumption of salt wedge conditions. Initially, the SFI is identified through vertical profiling with spatial resolution of 20 cm. Following this initial detection, the probe was positioned at fixed depth $d = -1.0$ m a.s.l. within the freshwater layer, where 120 continuous measurements of T and EC were recorded over a 1-hour period. The same sampling protocol was subsequently repeated in the transition zone at a depth of −3.5 m a.s.l. and in the seawater layer at a depth of −5.5 m a.s.l. With 120 T and EC values observed in each of three layers, coupled by the visual inspection of the water column, mean and standard deviation values of both, T and EC have been determined. T and EC characterising upper layer did not vary significantly over the 1-hour period of continuous observation ($\sigma_T = \pm 0.2^{\circ}$C and $\sigma_{EC} = \pm 0.9$ dS m^{-1}). Similar T and EC features have been determined for the bottom seawater layer ($\sigma_T = \pm 0.22^{\circ}$C and $\sigma_{EC} = \pm 1.3$ dS m^{-1}). For consecutive T and EC observations at fixed depth within the transition (SFI) zone, values of EC ranged from 15 to 45 dS m^{-1}, unless T values shown minor fluctuations ranging between 21.1 and 21.8 °C, indicating significantly lower uncertainty level in the SFI determination based on the T indicator, rather than the EC.

To ensure the insight to SFI dynamics and further improve the upstream freshwater discharge assessment characterizing the salt wedge, novel multilevel T sensing monitoring setup has been planned, developed and implemented at the Metković bridge profile for

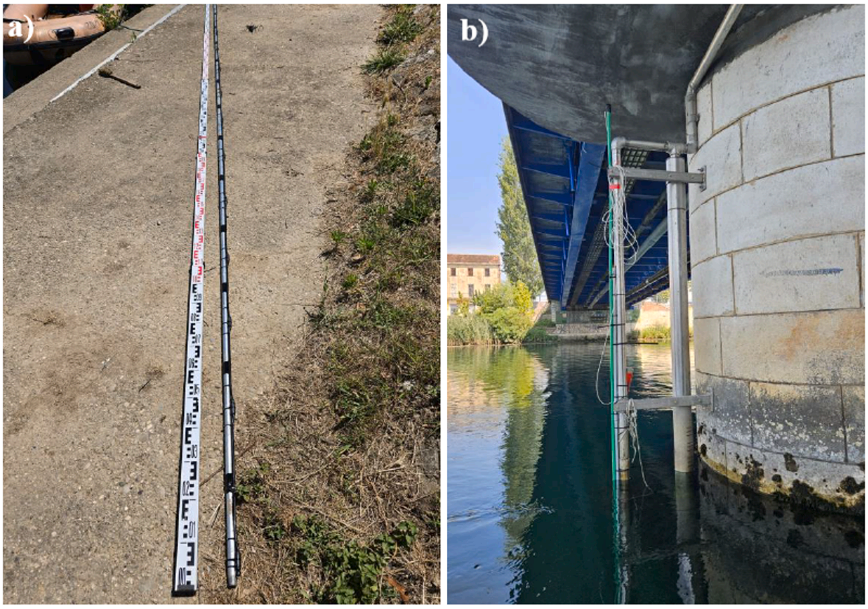

Fig. 3. a) Developed temperature chain consisting of 11 DS18B20 sensors at 40 cm equidistant intervals and b) installed temperature chain at Metković bridge pier in operation.

the purpose of this study. T monitoring setup includes a T sensor chain fixed to the bridge pier downstream, designed and installed to observe vertical T distribution of the water column and enable the insight to the position, shape and thickness of the SFI. Developed chain consists of in total 11 DS18B20 T sensors with ±0.3°C accuracy along the operative interval of −10° C to + 85 °C, distributed at equidistant 40 cm intervals with a sampling frequency corresponding to 15 min covering for water column depths of −1.1 to −5.1 m a.s.l. (Fig. 3).

Data sets from T sensors chain have been transmitted in real time to internal cloud thus enabling real time follow up of the operational functionality and continuity of the data set during September 4th−14th 2024 period.

2.3. On site implementation and data acquisition

To support the T based SFI monitoring, additional monitoring infrastructure has been used to observe for tidal, hydrological and local thermohaline features data sets in River Neretva estuary during the eleven-day period, September 4th−14th 2024. Monitoring system includes Adriatic Sea surface level and River Neretva surface level observation, River Neretva water column EC and T observations at two fixed depths and River Neretva stream velocity (U) observations at Metković bridge profile.

Tidal gauge is installed 2 km to the south east from the River Neretva mouth to observe for sea level oscillations (h_{SL}) while River Neretva surface level ($h_{Metković}$) is observed at the Metković bridge limigraph station located approximately 50 m downstream from the Metković bridge profile (Fig. 1). Both h_{SL} and $h_{Metković}$ are observed at 15-minute intervals using a THALIMEDES OTT water level logger matching the T chain sampling frequency and referring to the CET origin time. The device features operational range of ±19.999 m, a resolution of 0.001 m and an accuracy of ±0.002 m.

Probes at two depths (−0.37 and −5.4 m a.s.l.) observed continuously River Neretva water column EC and T at the Metković bridge profile. Upper probe is MANTA 2 40 + gauge with EC operational range of 0–100 dS m^{-1}, accuracy of ±1% and 0.0001 dS m^{-1} resolution standardized to 25 °C. T sensor operational range is −5–50 °C with a resolution of 0.01 °C and an accuracy of ±0.1 °C. Bottom probe is TruBlue CTD 585 with EC accuracy of 1% or 0.02 dS cm^{-1} along the range of 0.005–100 dS m^{-1}. T is observed with accuracy of ±0.2 °C in the range of 0–50 °C. Both probes were set up to a sampling frequency corresponding to 15 min.

River Neretva stream velocity is observed by three Channel Master H-ADCP's, each covering for one section of the Metković bridge profile. The H-ADCP velocity range corresponds to ± 20 m s^{-1} with accuracy of ±0.5% of observed velocity. H-ADCP installed at right section of Metković bridge profile covers total river profile horizontal width of 39.3 m discretised with 30 cells and 2 m blank distance. The setup is done in the same manner for the left section covering in total 39.6 m horizontal width discretised in 30 cells with 2 m of blank distance. Mid-section H-ADCP covers for 45 m of the river cross section width discretised in 20 cells and 1 m of blank space. Stream velocities obtained in this way represent mean values over the H-ADCP bar at a fixed depth consisting of respectively, 30, 20 and 30 cells. H-ADCPs were positioned at 0.19, 0.21 and 0.18 m a.s.l. for left, middle and right section respectively, with sampling interval of 25 s thus resulting in $U_{left,}$ U_{middle} and U_{right} stream velocities (Fig. 4).

A detailed survey of the River Neretva riverbed geometry at the Metković bridge profile has been conducted in September 2023 by simultaneous application of multibeam sonar and RiverPro ADCP. Maximum depths corresponding to the left, middle and right profile sections equal −4.92, −8.56, and −5.46 m a.s.l. respectively (Fig. 4). The total riverbed width observed hereby equals to 140.0 m. All depth and elevation values in this paper refer to the "Nula Trsta" vertical datum.

Initially, River Neretva discharge values have been up taken from the Croatian Meteorological and Hydrological Service (DHMZ), assessed from the mean stream velocity obtained by three H-ADCP's observations, profile geometry and observed $h_{Metković}$. It is important to emphasize the discharge assessment hereby has been adjusted and calibrated during mid and high-discharge occurrence thus offering not reliable discharge determination in case of stratified water column conditions found during low discharge occurrence. As the discharge reduces below 300 m^3 s^{-1}, depending on the mean sea level and tidal cycle occurrence, water column at the Metković bridge becomes stratified (Ljubenkov and Vranješ, 2012). The latter leads to the deflection from accurate freshwater discharge assessment due to the phenomenon of stratification in thermohaline features and upstream flow direction of the bottom seawater layer.

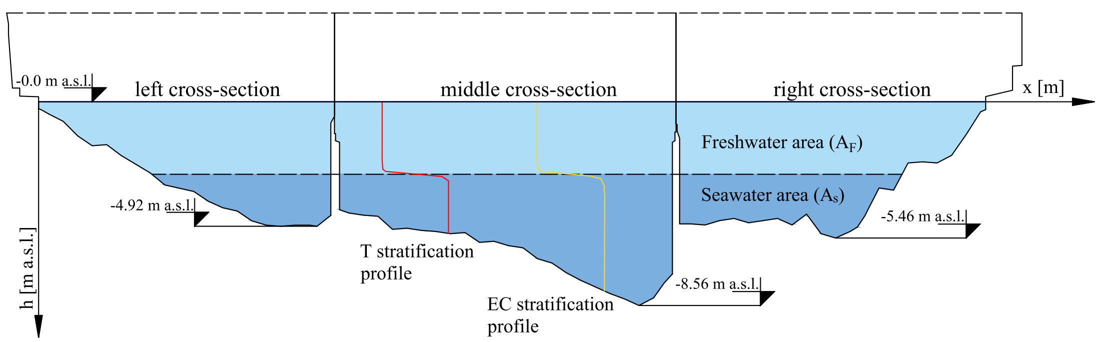

Fig. 4. Metković bridge hydrological profile geometry with three cross-sections (left, middle and right), seawater cross-section area A_S, freshwater cross-section area A_F, and EC and T schematic stratification along the water column.

2.4. Data processing

Relying on significant dependency of EC and T in natural environments (Hayashi, 2004), absolute vertical SFI position (h_{SFI}) has been determined from the T chain observations. Once data sets for each time increment are observed by the T chain, h_{SFI} is determined based on the vertical difference of the T observed. Freshwater upper layer of the salt wedge water column is assumed to be characterised by minor change in T which is verified from Neretva profiling results performed by Seba KLL-Q-2 portable probe during one-hour period of September 5th 2024. Deeper inspection of T demonstrates total T change along the upper freshwater layer does not fluctuate more than ±0.2 °C. Once the insight to all T values from sensor chain is enabled, the h_{SFI} corresponds to the depth of the upper of two neighbouring T sensors characterised by relative change of T higher than 0.5 °C.

Although the vertical resolution of T corresponds to 40 cm sensor spacing, observed time series enable the insight to the stratification since the profiling obtained SFI thickness is characterised by spatial scale greater than the sensor spacing (FGAG, 2023). Once h_{SFI} is defined, Matlab implemented Fast Fourier Transform (FFT) (Krishna, 2017) is applied to ensure smooth continuous representation of the T based h_{SFI} variation. From this point on, h_{SFI} corresponds to vertical position of SFI determined by newly developed T based monitoring and processed by the FFT.

2.4.1. Upstream freshwater discharge determination

The total wetted cross-section area (A_0) at Metković bridge profile is determined from observed $h_{Metković}$ and riverbed geometry. h_{SFI} is used afterwards to estimate the seawater cross-section area (A_S) while the freshwater area (A_F) is obtained as the difference between the A_0 and A_S (Fig. 4) as shown in Eqs. (1–5). The repetition of the procedure is applied to left, middle and right Metković bridge profile implying the h_{SFI} obtained from the T chain:

$$A_0^i = \int_0^{x^i} h(x^i)dx \tag{1}$$

$$A_0 = \sum_{i=1}^{n} A_0^i \tag{2}$$

$$A_S^i = \int_0^{x^i} (h(x^i) - h_{SFI})dx \; \forall \; |h(x^i)| > |h_{SFI}| \tag{3}$$

$$A_S = \sum_{i=1}^{n} A_S^i \tag{4}$$

$$A_F = A_0 - A_S \tag{5}$$

where *i* denotes the cross-section index, *h* represents the water depth at distance *x* for each cross-section *i* and *n* is the total number of cross- sections found at the profile.

Once A_F is known, H-ADCP obtained stream velocities for each Metković bridge profile sections are used to determine the total freshwater discharge Q_F (Eq. (6))

$$Q_F = \sum_{i=1}^{n} A_F^i \bullet U^i \tag{6}$$

where U_i represents (m s^{-1}) profile section stream velocity and A_F^i (m^2) represents specific profile section areas as shown in (Fig. 4).

2.4.2. Stratification parameters

Water column stratification is assessed via the dimensionless stratification parameter (n_s) based on the water column salinities (Hansen and Rattray, 1966):

$$n_s = \frac{\partial S}{S_0} = \frac{S_{bottom} - S_{surface}}{0.5 \bullet (S_{bottom} + S_{surface})} \tag{7}$$

where S_{bottom} and $S_{surface}$ (g l^{-1}) represent salinities at the bottom and at the surface of the Neretva water column. Unless n_s values lower than 0.1 characterise fully mixed water column, n_s value greater than unity demonstrate salt-wedge presence (Haralambidou et al., 2010).

The internal freshwater Froude number (Fr) (Geyer and MacCready, 2014) is determined by Eq. (8):

$$Fr = \frac{U}{\sqrt{g \bullet \Gamma \bullet h'}} \tag{8}$$

where U is longitudinal velocity (H-ADCP available) (m s^{-1}), g is the acceleration due to gravity (m s^{-2}), Γ is ($\Delta\rho/\rho_{bottom}$), Δρ is the bottom to surface density difference ($\rho_{bottom} - \rho_{surface}$) (kg m^{-3}) and h` is depth of the SFI or simply vertical difference between the

$h_{Metković}$ (m a.s.l.) and h_{SFI} (m a.s.l.). Fr number between 0.1 and 1.0, based on mixing number, defines salt wedge (Geyer and MacCready, 2014).

The input for Fr and n_s is obtained from the T, EC, ρ and S water column profiling results, performed six time per year during dry period from 2019 to 2023 using SEBA KLL-Q−2 multi-parameter probe at Komin and Opuzen profiles, located 9 and 12 km upstream from the river mouth respectively. Profiling results ensured the definition of functional interdependence between the EC and S as well as EC and ρ thus enabling the Fr and n_s determination from continuous EC and T observations obtained at Metković bridge profile.

2.4.3. Seawater freshwater interface decomposition

Amplitude spectral density (ASD) was computed by Matlab as the square root of the single-sided power spectral density (PSD) obtained from the FFT of the detrended time series, normalized by frequency bin width $\Delta f = Fs/L$ (where $Fs = 4$ samples h^{-1}). Normalized ASD is computed by dividing the ASD by a characteristic scale of the signal, such as its root-mean-square (RMS) value, standard deviation, or maximum amplitude. The normalized ASD is given by Eq. (9):

$$A_{norm}(f) = \frac{A(f)}{\sigma_x} \tag{9}$$

where σ_x is standard deviation of the time series ensuring $A_{norm}(f)$ is dimensionless.

To determine main driving forces controlling the h_{SFI} and their partial contribution identified by the normalised ASD inspection, time series were decomposed into two components, trend corresponding one and residual component covering for high frequency fluctuations so the h_{SFI} (m) is contributed as:

$$h_{SFI} = h_{SFI}^{trend} + h_{SFI}^{residual} \tag{10}$$

Trend component in Eq. (10) is determined as a moving average in order to eliminate all high-frequency oscillations and to identify trend features in h_{SFI} nature, unless the residual component represents the contribution of the lower than moving average time scale corresponding to external forces controlling the SFI dynamics. The moving average is defined by selecting an equal number of data preceding and succeeding a central value within a specified time span and calculating the arithmetic mean (Hansun, 2013). The residual component is subsequently obtained by eliminating the trend value from the corresponding observed time series.

2.4.4. Cross correlation analysis

Cross-correlation analysis has been applied to quantify the relationship between two-time series with emphasis to the internal time lag between two-time series of interest. The cross-covariance function $C_{xy}(k)$ (Thomson and Emery, 2014) is defined as:

$$C_{xy}(k) = \frac{1}{N-k}\sum_{i=1}^{N-k}(y_i - \overline{y})(x_{i+k} - \overline{x}) \tag{11}$$

where x_i and y_i are time series (with their respective units) at time i, N (–) is the length of the time series and k is the time lag.

The cross-correlation function ρ_{xy} [-] is defined as:

$$\rho_{xy} = \frac{C_{xy}(k)}{\sigma_x \sigma_y} \tag{12}$$

where σ_x and σ_y are the standard deviations of x and y time series. This approach enables the identification of time lags defining the temporal interdependence of time series of interest. Cross-correlation has been applied to both observed and residual time series (Box et al., 2016).

2.4.5. Linear regression analysis

A standard linear regression model assumes a linear relationship between a dependent variable Y and one or more independent variables X (Montgomery et al., 2021). In its simplest form, the model is given as:

$$Y = a + bX \tag{13}$$

where a is the slope and b is the y-intercept, both defined by minimising least squares between observed and regression model obtained values. Regression model fit quality is assessed by the coefficient of determination R^2:

$$R^2 = 1 - \frac{\sum_{i=1}^{n}(y_i - \widehat{y}_i)^2}{\sum_{i=1}^{n}(y_i - \overline{y}_i)^2} \tag{14}$$

where y_i is observed value for the i-th data point, $\widehat{y}_i$ is predicted value from the regression model for the i-th data point, $\overline{y}_i$ is the mean of observed values while the n (-) is the number of the data.

Linear regression cross correlation analyses are applied to available time series to obtain potential functional relationships and time lags in between data sets covered by the study (Vallejos et al., 2015).

2.4.6. Model performance metrics

Once the h_{SFI} is obtained from the linear regression model (Eq. 13) for the cross correlation determined time lag, model performance parameters RMSE and coefficient of efficiency CE have been applied to determine the fit quality of modelled h_{SFI} to mimic observed $h_{SFI.}$ RMSE defines quadratic mean of the differences between the observed and modelled h_{SFI} values by Eq. (15),

$$RMSE = \sqrt{\sum_{i=1}^{n} \frac{(h_{SFI,i} - \widehat{h}_{SFI,i})^2}{n}} \tag{15}$$

while CE in Eq. (16) estimates fit adequacy with unity values defining the perfect model capacity to mimic observed h_{SFI} values.

$$CE = 1 - \frac{\sum_{i=1}^{n} (h_{SFI,i} - \widehat{h}_{SFI,i})^2}{\sum_{i=1}^{n} (h_{SFI,i} - \overline{h}_{SFI,\,i})^2} \tag{16}$$

In Eqs. (15) and (16) $h_{SFI,i}$ (m) is the observed h_{SFI} value at time increment i, $\widehat{h}_{SFI,i}$ (m) is the modelled h_{SFI} at time increment i while $\overline{h}_{SFI,\,i}$ (m) represents observed mean value with n (-) equals number of available data.

2.4.7. SFI dynamics driven by upstream freshwater discharge and tides

After decomposing Q_F, h_{SL}, and h_{SFI} into their respective trend and residual components, similarities in the derivatives of the time series has been analysed to characterise the $h_{SFI,}$ dynamics. First order derivatives for the trend and residual Q_F, h_{SL}, and h_{SFI} components are determined:

$$\frac{\Delta y}{\Delta t} \approx \frac{y_{i+\Delta t} - y_i}{\Delta t} \tag{17}$$

where y_i is the time series value of variable of interest y at the time increment i, while $y_{i+\Delta t}$ is the neighbouring value.

Positive derivative value indicates an increase in the observed value unless negative value indicates a decrease. For both h_{SL} and h_{SFI}, positive and negative derivative values correspond to the rising (flood) and falling (ebb) stages of the tide, respectively. The increase in the Q_F results in the negative h_{SFI} derivative and vice versa.

2.5. Methodological assumptions

Following the methodological overview, we summarize and elaborate on relevant assumptions made in this study.

2.5.1. Water column delineation criterion

Vertical temperature difference of 0.5°C is adopted as a threshold to delineate the transition zone from and the freshwater layer in the River Neretva estuary with final goal to be used in the Q_F determination. This threshold is based on an assumption derived from a series of water column profiling conducted at the Metković bridge hydrological profile. Results obtained from profiling highlight no significant variations in T within the freshwater layer. Furthermore, continuous T values observed at a fixed depth of the transition zone fluctuated between 21.1 and 21.8 °C (Fig. 2) while the standard deviation of T observed in freshwater layer equals to $\sigma_T = \pm 0.2$°C. Since the T difference within the transition zone exceeds T difference characterising freshwater layer, T gradient corresponding to 0.5°C has been defined as threshold to delineate freshwater layer from the total water column.

2.5.2. Uniform velocity distribution within the freshwater layer

Vertical homogeneity of the stream velocity along the freshwater layer has been assessed from the analysis of the observed velocity profiles obtained by the RiverPro ADCP at Metković bridge profile. Profiling has been performed with the vertical resolution of 32 cm on October 21st 2025 during dry conditions along the mid-section of the Metković bridge. Stream homogeneity throughout the freshwater layer was evaluated using the coefficient of variation (CV) calculated from randomly selected transect velocity profiles. Obtained CV values indicate minimal vertical variability (ranging from 0.025 to 0.033) in stream velocity, highlighting the minimization of stream velocity vertical variations.

2.5.3. Temperature chain sensor vertical discretisation

The development and implementation of the novel temperature-based monitoring system has been based on prior knowledge of the position and vertical stratification characteristics of the River Neretva water column at several profiles downstream from the Metković bridge profile. Initial assumptions regarding the stratification structure were based on water column profiling conducted at the Opuzen and Komin monitoring profiles (FGAG, 2023). Based on data collected during a 5-year monitoring period, the transition zone width was estimated to be not below 0.4 m. This estimation served as the basis for setting up vertical spacing of sensors within the T chain, which was consequently set to 0.4 m to ensure adequate resolution to capture for transition zone. Data collected by T chain system demonstrated selected 0.4 m sensor spacing effectively captures temperature variations within the thermocline, supporting the initial assumption of the width of the transitional zone.

3. Results

3.1. Monitoring obtained data sets

A comprehensive overview of time series obtained by monitoring infrastructure is shown in Fig. 5 and Fig. 6. All time series used within this paper have been observed for the same time span corresponding to period of September 4th−14th 2024 with 15 min sampling rate and no missed values reported along the period.

Observed values of $h_{Metković}$ and h_{SL} during the reference period reveals notable similarities in both frequency and amplitude (Fig. 5a). The similarity in semidiurnal and diurnal tidal components in the $h_{Metković}$ signal compared to h_{SL} clearly indicates the upstream propagation of tidal effects from the river mouth with time lag of $h_{Metković}$ not larger than 20 min relative to h_{SL}. Residual values calculated as a difference between $h_{Metković}$ and h_{SL} indicate the direction of the River Neretva flow is downstream from the Metković bridge to the Adriatic Sea during the analysed period.

Stream velocity values in Fig. 5b reveal similar patterns across three profile sections, with absolute values for the left profile section consistently exhibiting lower mean compared to middle and right section. The influence of backwater effect from the Adriatic Sea is evident in the observed velocity patterns, with maximum stream velocities during the low tide, and minimum stream velocities occurred during high tide, with on average time lag not greater than 3 h (Figs. 5a and 5b). No negative stream velocities have been observed during the period of interest thus supporting the residual values in Fig. 5a.

Bottom probe observed EC in between 50.39 and 57.69 dS m^{-1} indicating presence of seawater at Metković bridge profile during the isolated event September 4th – 14th 2024 (Fig. 6a). Upper probe EC values do not exhibit values higher than 4.61 dS m^{-1} revealing the presence of freshwater upper layer with minor changes in EC due to the contribution of SFI lifting upwards. T values observed at bottom probe are stable with range between 24.14 and 25.17 °C while upper probe T values indicate the external influence leading to the T range between 15.5 and 20.4 °C.

Fig. 6b offers the insight to five vertical T profiles obtained by newly installed T chain. T profiles give insight to water column stratification properties and the T chain capacity to capture for SFI features for the dates September 6th, 8th, 10th, 12th and 14th 2024,

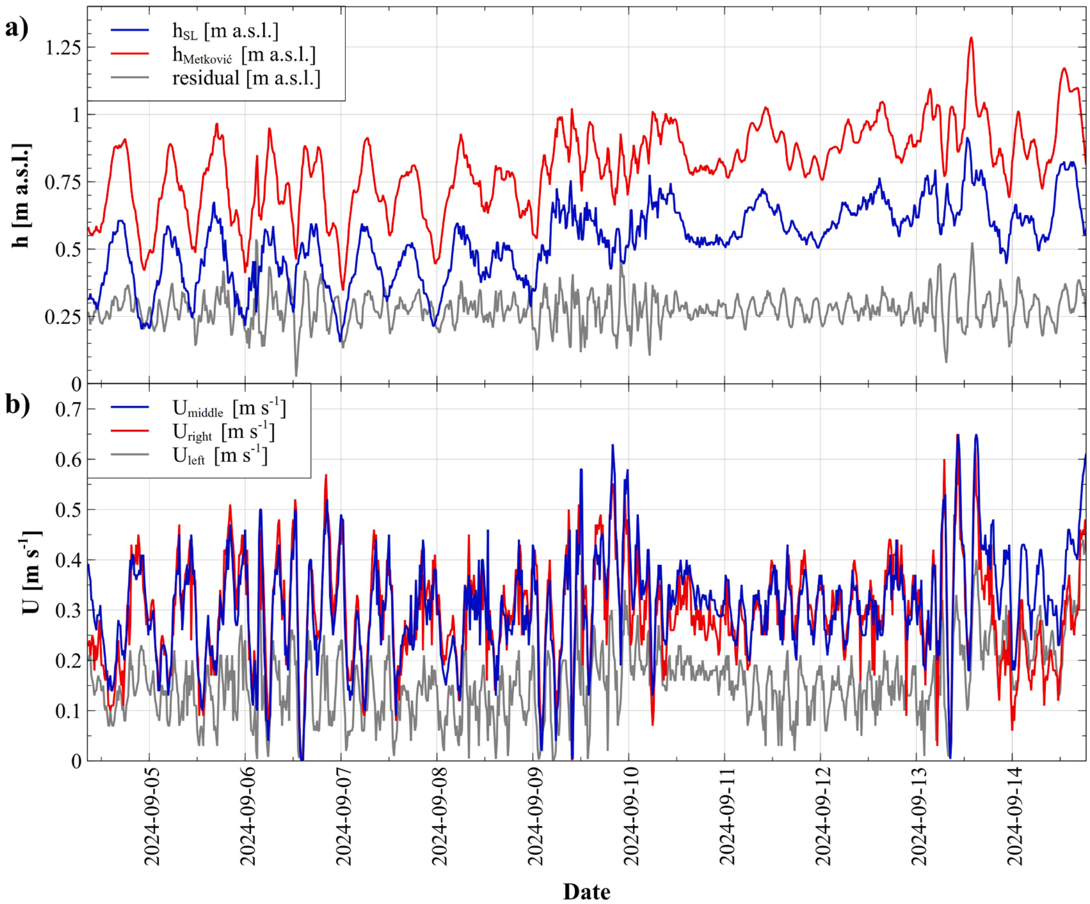

Fig. 5. Observed values of a) h_{SL}, $h_{Metković}$ and their residual b) River Neretva stream velocities for left, middle and right cross-section (U_{left}, U_{middle} and U_{right}) for the period September 4th −14th 2024.

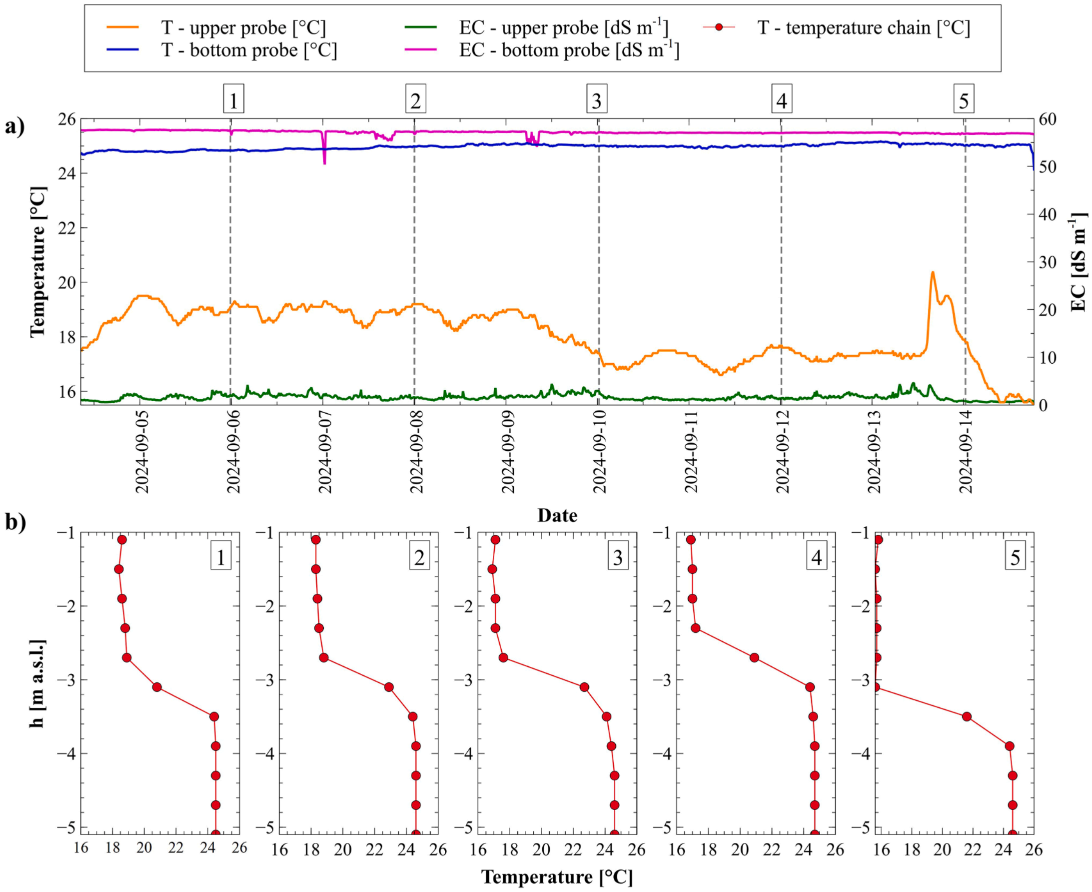

Fig. 6. a) EC and T time series obtained at upper and bottom probe at Metković bridge profile for the period September 4th – 14th 2024; b) T chain obtained T profiles for time increments marked on a).

at 12:00 PM. T profiles exhibit a pronounced vertical gradient with lower T values observed within the upper layer and increase in T downwards with depth. T observations obtained from both monitoring systems demonstrate significant degree of matching with on average deviations of 0.14 °C and 0.24 °C for upper layer and bottom layer T values, respectively. The h_{SFI} is defined as the depth of the uppermost T sensor in the sensor chain exhibiting T difference greater than 0.5 °C between two neighbouring consecutive sensors as explained previously.

3.2. Seawater-freshwater interface and freshwater discharge features

The h_{SFI}, as determined from the installed T chain sensors, ranged between −1.5 and −3.9 m a.s.l. during analysed period and exhibited near stepwise pattern corresponding to salt wedge conditions (Fig. 7a). It is important to note the SFI width is shown to be larger than T sensors internal displacement, confirming the 40 cm as an appropriate spatial resolution for T profiling hereby (Fig. 6b). Continuous representation of h_{SFI} variations is ensured by the FFT application to raw data set. The coefficient of determination (R^2) between the observed h_{SFI} and the FFT one equals 0.86 (Pearson correlation coefficient r = 0.93), indicating significant fit quality and relevant representation of observed data set.

Total wetted cross-section water area (A_0) at Metković bridge profile is composed of seawater cross-section area (A_s) and freshwater cross-section area (A_F). Values of total (A_0) and seawater (A_s) cross-section areas were determined by Eqs. (1) and (3) based on Metković bridge surface water elevation $h_{Metković}$, h_{SFI} and profile geometry. Once A_0 and A_s are known, A_F is derived from Eq. (5). The inspection of geometric cross section areas A_0, A_s and A_F time series in Fig. 7b lead to the fact the h_{SL} dominantly defines the A_0 since its influence to $h_{Metković}$. Periodic nature of A_S is similar to h_{SFI} as expected from Eq. (3). The change in A_S and A_F is reciprocal and can be explained by simultaneous effects of h_{SL} and Q_F and their partial contribution to h_{SFI} position. As the high tide occurs, $h_{Metković}$ increases as well as the h_{SFI}, leading consequently to the increase in both A_S and A_0 with no significant increase in Q_F. Fig. 8 demonstrates the dominance of the h_{SFI} in A_F definition. Once the Q_F is increased, A_0/A_F is decreased and vice versa, whose physical justification is found in stratification diminishing as the upstream freshwater discharge increases (Cardona et al., 2025) and h_{SFI} is pushed towards the riverbed bottom due to the forcing of the upstream inflow (Fig. 7a) thus reducing the A_S. Inspection of the period with increase of Q_F trend highlights the decrease of both h_{SFI} and A_S in Fig. 7b and c.

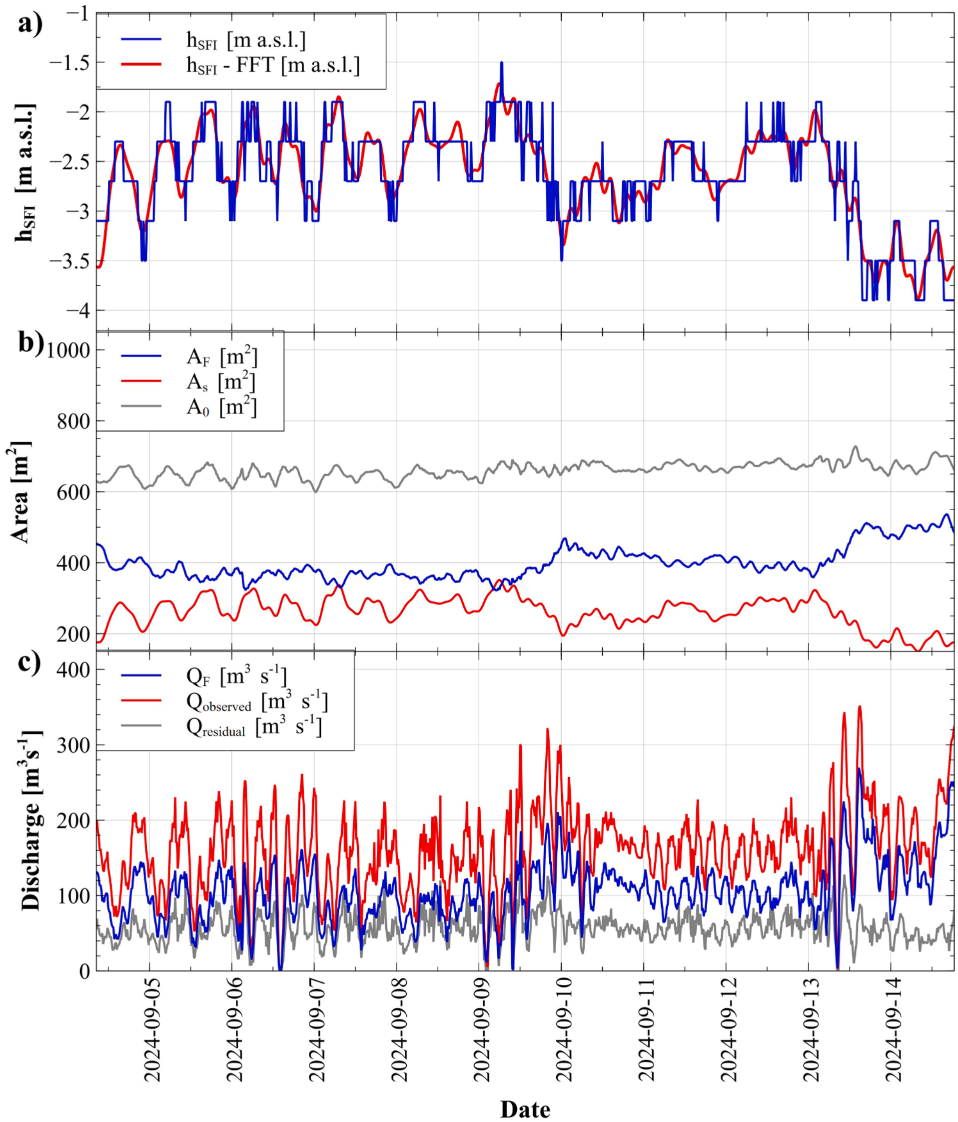

Fig. 7. Time series of a) observed and FFT obtained h_{SFI}, b) total (A_0), seawater (A_S) and freshwater (A_F) cross-section area at Metković bridge profile, c) freshwater discharge (Q_F), observed discharge ($Q_{observed}$) and their residual ($Q_{residual}$) respectively.

Based on the defined A_F and the corresponding stream velocity values, the Q_F was calculated by Eq. (6). Q_F derived from the difference between A_0 and A_s represents the flow of the freshwater within the upper freshwater layer. It remains influenced by tidal dynamics, as its computation is based on surface stream velocity data obtained from the Metković bridge station. Q_F values for the observed period ranged between 0.87 and 269.55 $m^3 s^{-1}$, representing a favourable setting for seawater intrusion. Since the amount of 40 $m^3 s^{-1}$ represents the biological minimum of the Mostar HPP (40 km upstream), Q_F values found below 40 $m^3 s^{-1}$ for the reference period stem from the backwater seawater level influence to stream velocities at Metković bridge profile (Fig. 5a and b).

Given the evident tidal influence on surface water elevation at Metković bridge profile, Q_F values represent realistic freshwater upper layer discharge influenced simultaneously by tidal variations due to the backwater effects and upstream freshwater inflow thus enabling the insight to available freshwater discharge during highly stratified conditions characterising dry periods. However, during discharge increase periods (above 300 $m^3 s^{-1}$), the tidal signal in the $h_{Metković}$ diminishes, indicating a suppression of tidal effects under high-flow conditions.

3.3. Stratification parameters

During the observed period, n_s and Fr are determined and presented in Fig. 9c.

As a result of profiling along the Neretva estuary, relationship between S and EC and ρ and EC are shown at Fig. 9a and b. Significant

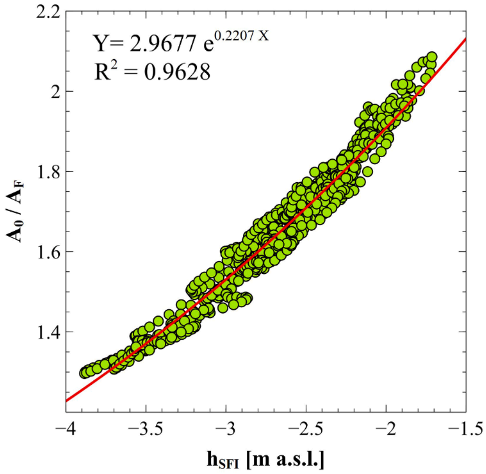

Fig. 8. Relationship between h_{SFI} and A_0/A_F with exponential relationship and coefficient of determination.

linear correlation in both cases ($R^2 = 0.9994$ between S and EC and $R^2=0.9941$ between ρ and EC) indicate interdependence between the variables where increase of EC leads to increase in S, same as with ρ values, and vice versa.

Values of the n_S exceed unity through the entire observation period, ranging from 1.75 to 2.02, indicating consistently strong

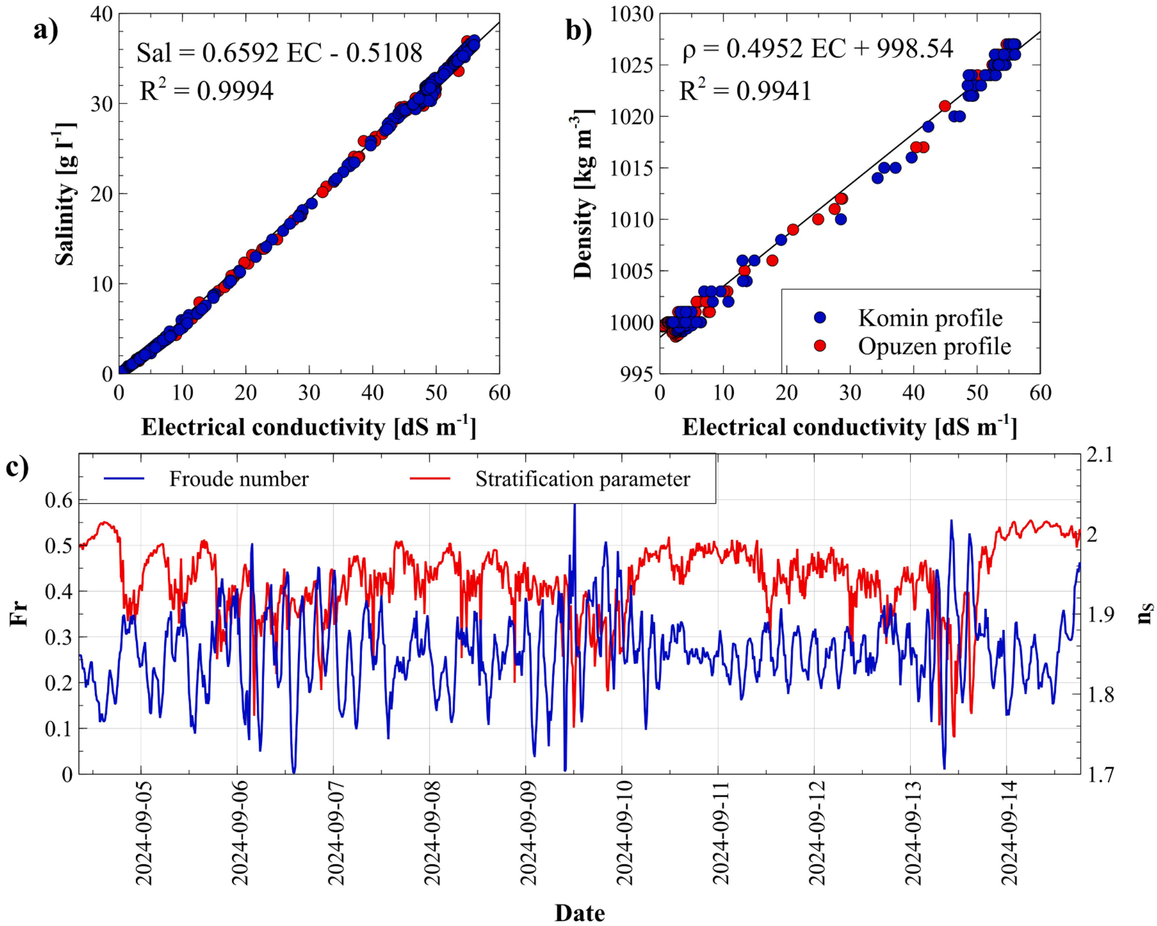

Fig. 9. a) Relationship between S ($g\ l^{-1}$) and EC ($dS\ m^{-1}$) on the left and ρ ($kg\ m^{-3}$) and EC ($dS\ m^{-1}$) on the right for water samples at Komin (blue) and Opuzen (red) profile for the period 2019–2023; b) Stratification parameter (n_S) and Froude number (Fr) for the period September 4th−14th 2024.

vertical density stratification characterising the salt-wedge conditions a found in estuary (Cordero-Acosta et al., 2024). Pronounced decrease in n_S is found during two isolated events on September 9th–10th and September 13th–14th characterised by the increase of the Q_F above 150 and 200 $m^3\ s^{-1}$ respectively. These changes indicate a reduction in stratification associated with increased freshwater discharge, which is in agreement with work by Postacchini et al. (2023).

The internal Fr ranged from 0.0025 to 0.59, supporting additionally the salt wedge interpretation of the Neretva estuary during the observed period. According to (Geyer and MacCready, 2014) Fr values found below unity are typical for stable, highly stratified salt-wedge conditions where buoyancy forces dominate over mixing.

Periods with a slight decline in n_s coincide with the highest observed Fr values, reflecting episodes of increased Q_F dominance. During these intervals, September 9th–10th and September 13th–14th, enhanced upstream flow weakened the density gradient and promoted partial mixing, although not sufficiently to disrupt the overall salt-wedge structure.

3.4. Frequency domain seawater-freshwater interface dynamic features

Normalized ASD plots are applied to h_{SL}, Q_F, U_{middle} and h_{SFI} time series to identify potential similarities in their frequency patterns. All variables of interest are characterised by the dominance of both diurnal and semidiurnal constituents (Fig. 10a). The latter is consequence of the fact that Metković bridge profile is located in the tidal backwater zone during the analysed period. Matching of Q_F and U_{middle} ASD functions relies in Eq. (6) where the stream velocity represents the first order data, thus defining the transient nature of determined Q_F (blue and green lines overlapping). To identify the dominant mechanisms governing the h_{SFI}, time series of Q_F and h_{SL} were decomposed into trend and residual components. Initially, the trend component was extracted by using a 24-hour moving average, effectively removing tidal fluctuations and leaving long-term trends. The residual component, representing all higher frequency variations, was obtained by subtracting the trend from the original time series.

Decomposition of h_{SL}, Q_F and h_{SFI} is shown of Fig. 11 while their normalized ADS plots are shown in Fig. 10b - d.

A comparative analysis of decomposed h_{SL}, Q_F and h_{SFI} time series and their ASD's indicates a predominant influence of Q_F to control h_{SFI} trend (Fig. 10 a, 10c, 11b and 11c).

The alignment of ASD for residual components of h_{SL} and h_{SFI} suggest that h_{SFI} oscillations are highly tide-driven with presence of both diurnal and semidiurnal constituents (Figs. 10c, 11a and 11c). Maximum contribution of h_{SL} to h_{SFI} has been identified during periods when the trend component of Q_F remained relatively stable (Fig. 11b). Along with diurnal and semi-diurnal constituents in h_{SL} and Q_F signals, independent high frequency peaks are notable at 0.25 cycles h^{-1}, indicating Q_F changes at 4-hour time scale.

To evaluate the influence of Q_F on h_{SFI}, a new trend and residual components were determined. 4-hour moving average, corresponding to the upstream HPP operational time increment, was applied to define trend component (Fig. 10d), while the residual was defined by subtracting the trend from the original time series as was done for daily trend above.

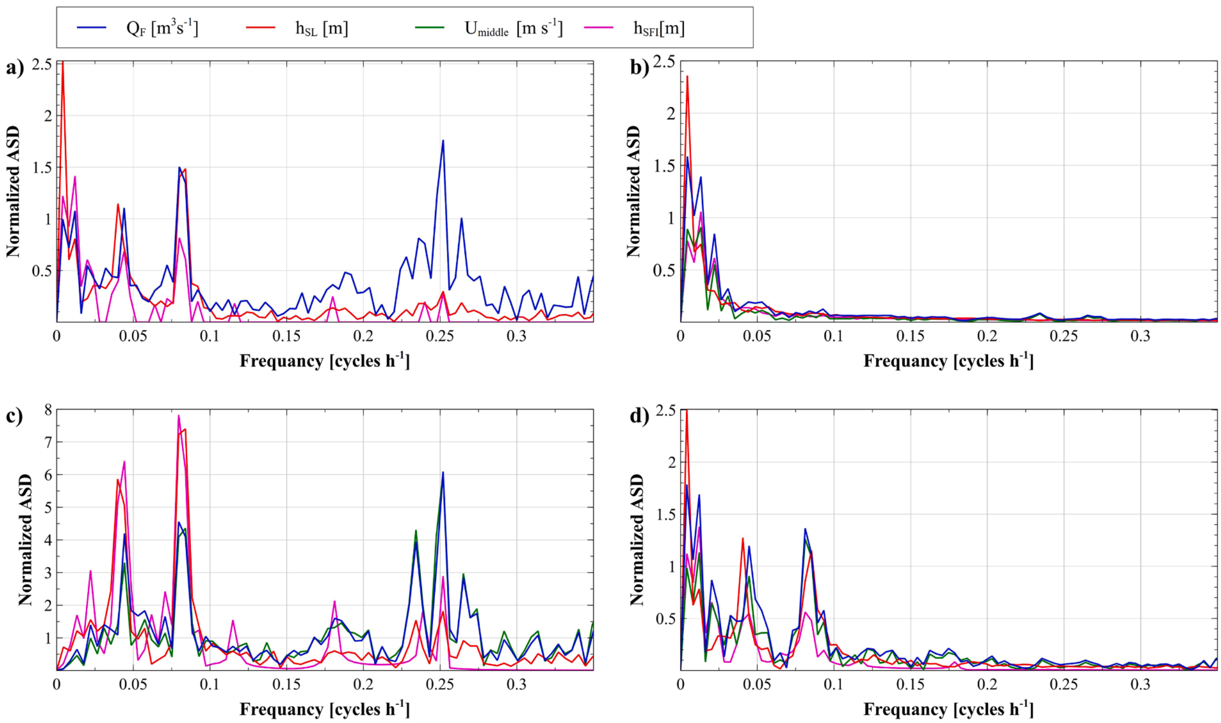

Fig. 10. Normalized ASD for a) observed time series, b) 24-hour moving average time series, c) 24-hour residual time series, d) 4-hour moving average time series for Q_F, h_{SL}, U_{middle} and h_{SFI}.

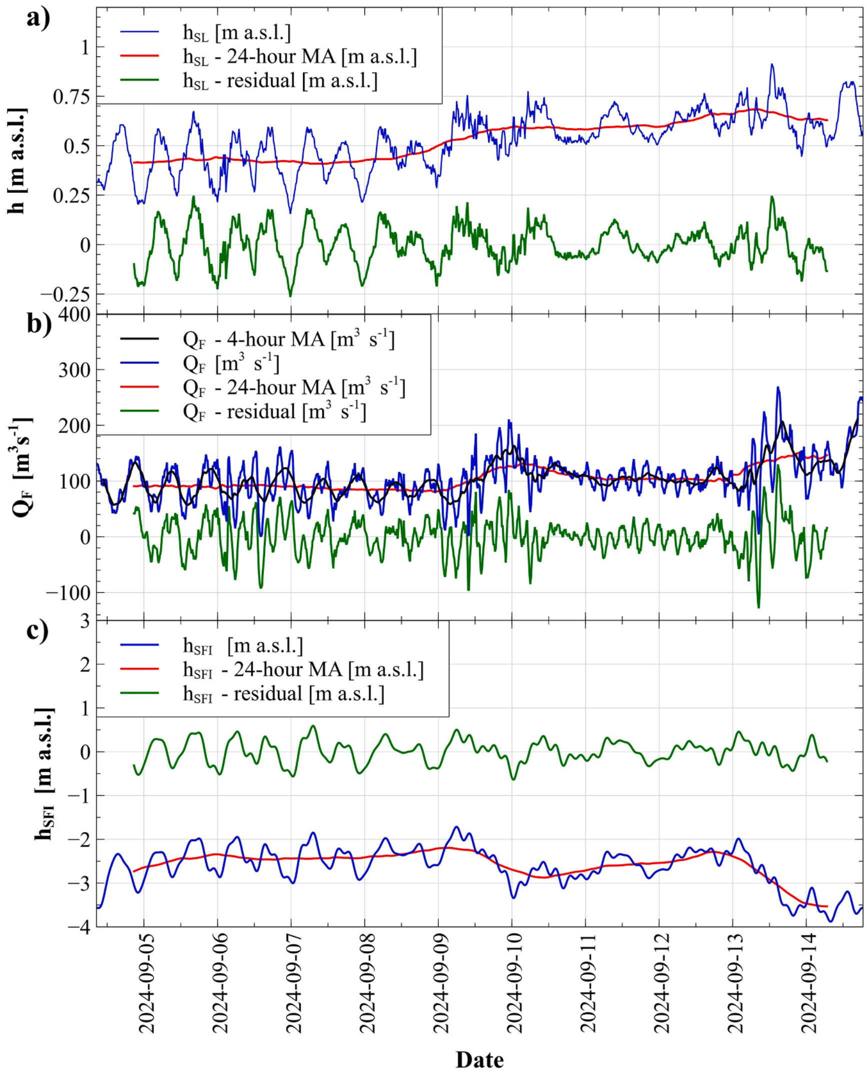

Fig. 11. Decomposition of observed time series to trend obtained by MA application and residual components for a) h_{SL}, b) Q_F and c) h_{SFI}.

Discharge peaks corresponding to higher frequencies indicate short-term variability associated with independent release events from the upstream HPP Mostar and Čapljina. Based on the dominant frequencies, the h_{SFI} time series was divided into two sub-periods: i) period dominated by tidal oscillations with a stable Q_F trend, assessed through the 24-hour trend and associated residual, and ii) period characterised by increased Q_F releases from the upstream HPP's.

Episodes affected by intensified Q_F releases are identified on September 9th (21-hour interval) and from September 12th to 13th (35-hour interval) with maximum 30 min' time lag between Q_F increase and h_{SFI} decline, based on cross-correlation analysis.

Further analysis is performed on two periods: i) periods dominated by the tides (from September 4th 2024 at 8:45 AM to September14th 2024 at 6:30 PM excluding ii)) and ii) periods dominated by upstream HPP Q_F release (from September 9th 2024 at 2:15 AM to September 9th 2024 at 11:30 PM and from September 12th 2024 at 6:30 AM to September 13th 2024 at 5:30 PM).

3.5. Seawater-freshwater interface assessment framework

Based on the methodology presented above and identified peculiarities on the h_{SL} and Q_F influence to h_{SFI} for observed period, it is possible to define the SFI forecasting assessment framework that could be used for h_{SFI} determination based on real time monitoring of h_{SL} and Q_F. Generally, it is possible to define h_{SFI} as:

$$h_{SFI} = h_{SFI}^{trend} + h_{SFI}^{residual} \quad (18)$$

$$h_{SFI}^{trend} = f\left(Q_F^{trend}\right) = A \bullet Q_F^{trend} + B \quad (19)$$

$$h_{SFI}^{residual} = f\left(h_{SL}^{residual}\right) = C \bullet h_{SL}^{residual} + D \quad (20)$$

The latter is applied to two identified periods: i) periods dominated by the tides (from September 4th 2024 at 8:45 AM to September 14th 2024 at 6:30 PM excluding ii)) and ii) periods dominated by upstream HPP Q_F release (from September 9th 2024 at 2:15 AM to September 9th 2024 at 11:30 PM and from September 12th 2024 at 6:30 AM to September13th 2024 at 5:30 PM). For the dominantly tidal driven period, h_{SFI} trend has been defined based on the Q_F trend, unless the tidal induced transience is introduced from the h_{SL} residual which is in compliance to ASD features (Figs. 10b and 10 c). During the periods characterised by the increased Q_F due to upstream HPP operational release, Q_F trend based on the 4-hour moving average application from Fig. 10d is used to mimic h_{SFI}. Linear regression is applied to both tidal dominated and discharge dominated periods to estimate unknown parameters in Eqs. (19) and (20), whose parameters are presented in Table 1.

Finally, h_{SFI} has been assessed by the implementation of Eqs. (19) and (20) into Eq. (18) to further support the hypothesis of simultaneous contribution of Q_F and h_{SL} on different time scales into the h_{SFI} definition. Results presented in Fig. 12, demonstrate strong agreement with the h_{SFI} obtained from T chain observations with a coefficient of determination of $R^2 = 0.861$, CE= 0.862 and RMSE= 0.152.

3.6. Seawater-freshwater interface assessment framework validation

To test the capacity and ability to define $h_{SFI,}$ presented assessment framework was validated for the time period from June 17th to June 24th 2025. One-week period included values of h_{SL}, $h_{Metković}$, U, EC and T at Metković bridge profile from the monitoring system with 15-minute sampling rate without missing data reported. Newly developed T chain system provided T values along water column for the same time period. The procedure of data processing explained under the Methodology section has been employed to new data set. Decomposition of verification period time series of h_{SL}, Q_F and h_{SFI} on trend and residual components has been carried out based on implemented normalized ASD analysis which confirmed the assumption used for development of assessment framework. Q_F is the main driving force defining the h_{SFI} trend, while the tidal components contribute to diurnal and smaller than daily h_{SFI} oscillations. During the validation period, no release from upstream HPPs is observed.

Based on the assessment framework, values for A, B, C and D parameters are determined by minimising RMSE from Eqs. (19) and (20).

$$h_{SFI} = h_{SFI}^{trend} + h_{SFI}^{residual} \quad (21)$$

$$h_{SFI}^{trend} = f\left(Q_F^{trend}\right) = -0.0157 \bullet Q_F^{trend} - 5.7685 \quad (22)$$

$$h_{SFI}^{residual} = f\left(h_{SL}^{residual}\right) = 2.5177 \bullet h_{SL}^{residual} + 0.0011 \quad (23)$$

Fig. 13 offers the insight to the comparison of h_{SFI} derived from T chain and h_{SFI} simulated by developed analytical framework. Results demonstrate agreement between simulated and observed values with a coefficient of determination of $R^2 = 0.772$, CE= 0.772 and RMSE= 0.169, demonstrating strong predictive capability and confirming the robustness of the proposed analytical approach.

3.7. Seawater-freshwater interface dynamics

To assess how Q_F and h_{SL} control the h_{SFI} dynamics, temporal derivations of the first order have been determined for Q_F, h_{SL} and h_{SFI} with emphasis to different time scales. As shown in previous chapter, during the tidal dominated period in controlling the $h_{SFI,}$ h_{SL} residual and Q_F 24-hour moving average have been set up to describe h_{SFI} transient nature. For the sub periods of h_{SFI} dominantly controlled by upstream HPP operational regime, mostly matching the 4-hour period, h_{SFI} is controlled by the Q_F 4-hour moving average. Strict insight to those sub periods is given in Fig. 14a and c. As shown in Fig. 14a, three grey areas denote the tidal dominated periods. Sub periods of Q_F four hour moving average defining the h_{SFI} are highlighted in Fig. 14c.

Inspection of h_{SFI} residual after eliminating daily trend by moving average application and its dependence to h_{SL} residual determined in the same manner as the h_{SFI} residual (Fig. 14b) highlights significant correlation based on in total 35 temporal increments characterising tidal dominated sub periods ($R^2 = 0.9375$, $r = 0.968$). The slope of linear regression with its positive value indicates rise of h_{SFI} during the flood tide and decline of h_{SFI} during the ebb tide.

Sub periods of the dominance of Q_F 4-hour moving average in defining the h_{SFI} 4-hour moving average (Fig. 14d), discover significant correlation defined on in total 11 temporal intervals with R^2= 0.9267 and $r = 0.963$ Hereby, negative slope of linear regression model indicates the decline of h_{SFI} during the Q_F increase and vice versa.

Table 1
Values of linear regression model coefficients defining trend and residual component of h_{SFI} obtained for the period September 4th –14th 2024.

Coefficient		A	B	C	D
	24-hour trend	−0.0154	−1.0467		
Q_F	4-hour trend	−0.0104	−1.2321		
h_{SL}	24-hour residual			2.2459	−0.0072

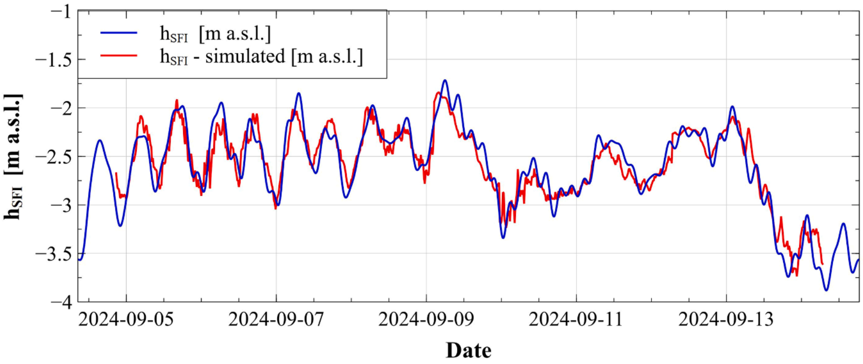

Fig. 12. h_{SFI} determined by T chain based monitoring system and h_{SFI} simulated by developed analytical framework (h_{SFI} – simulated).

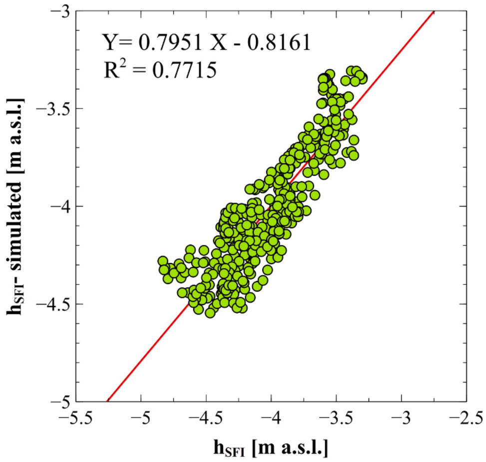

Fig. 13. h_{SFI} derived via FFT from temperature sensor measurements (h_{SFI}) and h_{SFI} simulated by developed analytical framework (h_{SFI} – simulated) for validation period.

The rate of change of the h_{SFI} corresponds the order of magnitude of tidal induced changes in h_{SL} (Fig. 14b) thus additionally confirming the tidal constituents' presence in h_{SFI} ASD pattern (Fig. 10b) and leading to the conclusion, tidal mechanism define the h_{SFI} transient nature on both diurnal and semidiurnal time scales. Apart from the tidal dominated period, the rate of change of ± 10 m^3 s^{-1} of Q_F 4-hour trend induced by the HPP operational regime upstream, causes the ± 0.1 m h^{-1} change in h_{SFI}.

4. Discussion

Main outcomes of this study, as shown in the Results section, can be summarised as follows: i) development and implementation of T based water column stratification monitoring with high efficiency in salt wedge estuaries application; ii) establishment of framework for the upstream freshwater discharge determination in highly stratified salt wedge estuaries as confirmed by ns and Fr, iii) identification of h_{SFI} as two main mechanism controlled parameter: Q_F and h_{SL} interplay defining h_{SFI} trend and residual transience and iv) establishment of simple linear model to define h_{SFI} based on available observations with high potential to be used as a forecasting framework. To further strengthen above findings, we further extend the analysis to ensure results relevance, validity and point out potential limitations as well as benefits of the study

4.1. T based salt wedge monitoring relevance, benefits and potential limitations

Along the Mediterranean, monitoring of estuarine fed groundwater systems have been implemented into different hydrogeological units along the coastal systems (Lovrinović et al., 2021; Tosi et al., 2025) emphasizing EC and T as variables of interest to capture for SWI transience. Same parameters have been observed by the implementation of cost effective automatic vertical profiling system in boreholes (Jeon et al., 2024). Profiling results from estuarine water column have been used for purpose of numerical models calibration and validation as shown in Krvavica and Ružić (2020) as well as Gaiolini et al. (2023) who used local salinity observation for purpose of Volturno river SWI analysis and model calibration. Wegman et al. (2025) used salinity measurements based on conductivity, temperature, and depth from (CTD) sensors monitoring at 20 locations in the Rhine-Meuse Delta estuary by applying a

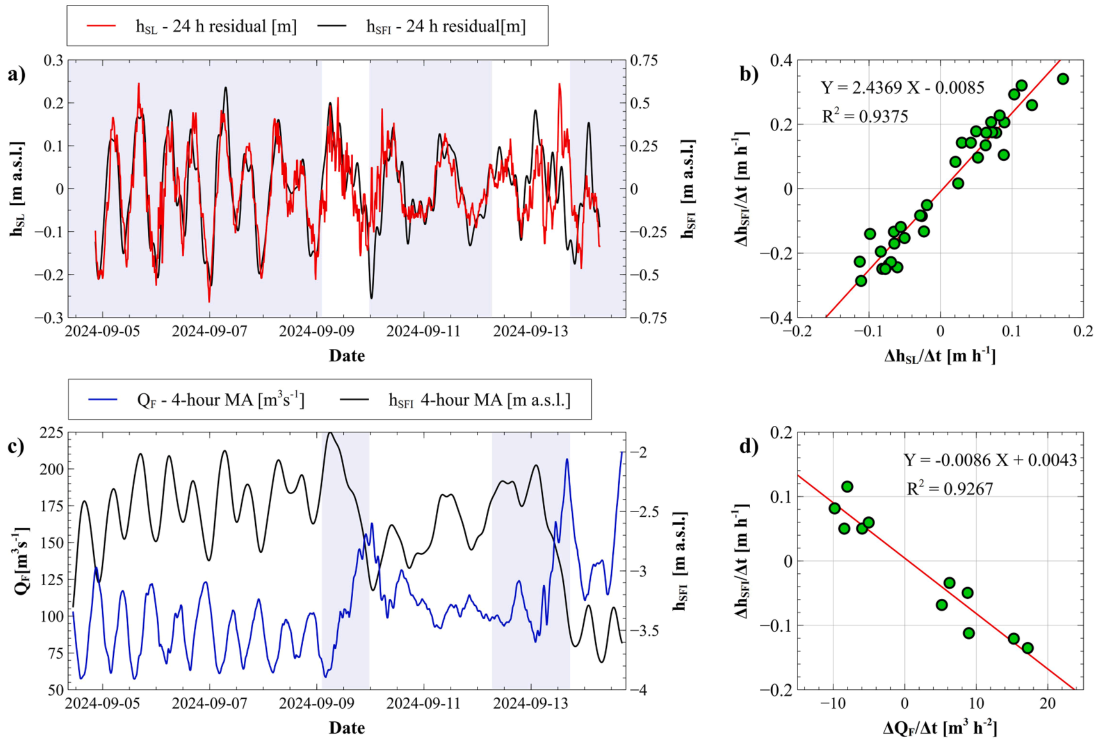

Fig. 14. a) Comparison of h_{SL} and h_{SFI} 24-hour residual component, b) temporal derivation scatter plot with linear regression for h_{SL} and h_{SFI} 24-hour residual, c) Q_F and h_{SFI} 4-hour trend component, d) temporal derivations scatter plot with linear regression for Q_F and h_{SFI} 4-hour trend.

multi-depth approach. The content above emphasizes the need for efficient and reliable monitoring of the SFI as an SWI parameter in estuaries. Implemented T chain presented in this paper and implemented at River Neretva estuary demonstrates the relevance and functionality not only during hydrological events with dominance of Q_F or h_{SL} in h_{SFI} definition, but also when simultaneous contribution of Q_F and h_{SL} in h_{SFI} definition is present. As shown in Fig. 11b, operational interval of the T chain in this study has been demonstrated between 0.87 and 269.55 $m^3\ s^{-1}$, unless h_{SL} extreme values correspond to 0.155 – 0.915 m interval (Figs. 5a and 11a). To further define the T chain operability, insights to Fr and n_S values in Fig. 9c point out monitoring period in this paper corresponds to highly stratified conditions with various effects of Q_F and h_{SL} in the definition of SFI zone depth, width and slope.

Primary study related limitation of the developed and implemented T based monitoring chain is the maximum deployment depth of the T sensor chain (–5.4 m a.s.l.) and the internal vertical sensor spacing of 0.4 m. Given that the maximum depth at the Metković bridge profile at the cross-section centre reaches –8.56 m a.s.l., variations in the h_{SFI} occurring below the lowest sensor were not detected but keeping on mind h_{SFI} did not fall below – 3.81 m a.s.l. over the study period of interest. The latter can be easily upgraded by the extension of the T chain thus covering for total water column. Internal T sensor vertical distance of 0.4 m has been selected by taking into consideration cost optimization and adjustment to SWI transitional zone width. As can be seen in Fig. 6b, even the 0.4 m set up internal distance covers for the T values within the thermocline. Further upgrade on the T chain can be easily performed by setting up smaller internal distance to capture for T changed in SFI characterised by smaller width transition zones.

Due to the usually high price met in environmental monitoring and constant need for system optimization in both, cost and efficiency (Abramic et al., 2014), T based monitoring system potentially overcomes price limitations present in EC, pH or salinity sensors. Using low-cost T sensors to continuously observe vertical T profiles within highly stratified water column in estuaries, presuming presence of T difference in upper freshwater and bottom seawater layer, could be an example of cost-effective procedure with capability in observing T vertical features.

4.2. Freshwater discharge assessment validation

To validate the Q_F assessment procedure presented in this paper, discharge data from the nearest upstream hydrological station Žitomislići, located in Bosnia and Herzegovina approximately 46.85 km from the mouth of the Neretva River (Fig. 1) were obtained.

Between these two stations, three tributaries contribute the Neretva River: Trebižat, Bregava, and Krupa, respectively. Trebižat presents a right-bank tributary, with discharge observed at the Humac hydrological station. Bregava and Krupa are left-bank tributaries with no discharge, but surface water elevation available. A schematic overview of the Neretva River's tributaries, hydrological stations, and the direction of flow is presented in Fig. 15. It is important to note Žitomislići station is excluded from the Adriatic Sea backwater zone and is not tidally influenced thus offering a reliable Q_F representing hydrological input downstream.

To overcome the absence of discharge observations at left bank tributaries, data from hydrological yearbooks covering the Adriatic Sea river basin district were examined and included in the analysis (Federalni hidrometeorološki zavod, 2022). Based on the available daily discharge values, the annual minimum, maximum, and mean discharge values for the Trebižat and Bregava tributaries are identified and presented in Table 2.

Table 2 highlights Trebižat and Bregava rivers seasonal variability, with Trebižat contribution dominantly in dry season (Bonacci et al., 2013).

The total freshwater discharge of the Neretva River upstream from the Metković bridge profile is defined as the superposition of the Žitomislići and Trebižat contribution and marked as $Q_{upstream}$. $Q_{upstream}$ data were obtained for the entire observation period on a 15-minute sampling rate. As shown in Fig. 16a, during the period September 4th −14th 2024, Trebižat discharge remained relatively constant, contributing with approximately 3–7% to the $Q_{upstream}$. Sudden increase in Žitomislići discharge values at September 9th 2024 at 9:30 AM and September 13th 2024 at 9:45 AM are attributed to Mostar HPP operating regime upstream.

Q_F obtained from Eq. (6) and the total discharge observed at the Metković bridge ($Q_{Observed}$), as provided by DHMZ, exhibit similar temporal oscillation patterns, with Q_F consistently being lower than $Q_{Observed.}$ This difference arises due to the background of both discharge values $Q_{Observed}$ and Q_F, relying on the same first order stream velocities U_{left}, U_{middle} and U_{right} (Fig. 5b). The determination of Q_F considers only effective freshwater cross-sectional area, defined as the difference between the total wetted and seawater cross-sectional area. In contrast, $Q_{Observed}$ is computed by using the entire wetted cross-sectional area without distinction between freshwater and seawater area, thus ignoring water column stratification. Consequently, $Q_{Observed}$ overestimates Q_F, whereas Q_F provides more accurate representation of the freshwater discharge in highly stratified conditions presence along the backwater zone of river Neretva estuary fulfilling closely the freshwater discharge mass conservation between Žitomislići and Metković bridge profiles with incorporation of left and right bank tributaries.

To validate Q_F and its superiority over $Q_{Observed}$ accuracy, a comparison of $Q_{upstream}$ and Q_F (Fig. 16b) revealed substantial differences in magnitude and oscillatory behavior. Oscillations of Q_F stem from tidally modulated velocities in the backwater zone at Metković bridge profile. The latter is entirely absent in the $Q_{upstream}$ confirming Žitomislići hydrological station remains beyond the reach of seawater backwater influence even during periods of low river flow and maximum salt-wedge intrusion.

The 24-hour trend component of the Q_F, obtained through MA application is compared to the upstream river discharge $Q_{upstream}$ to eliminate the direct influence of tidal dynamics (Fig. 16c).

Throughout nearly entire observed period, Q_F 24 h trend values exceed the $Q_{upstream}$. The difference is attributed to ungauged lateral inflows from tributaries and direct catchment inflow to the river Neretva between Žitomislići and Metković bridge profiles. During an extended low-flow period (from September 4th to September 9th 2024) in Fig. 16c, characterised by prolonged drought and

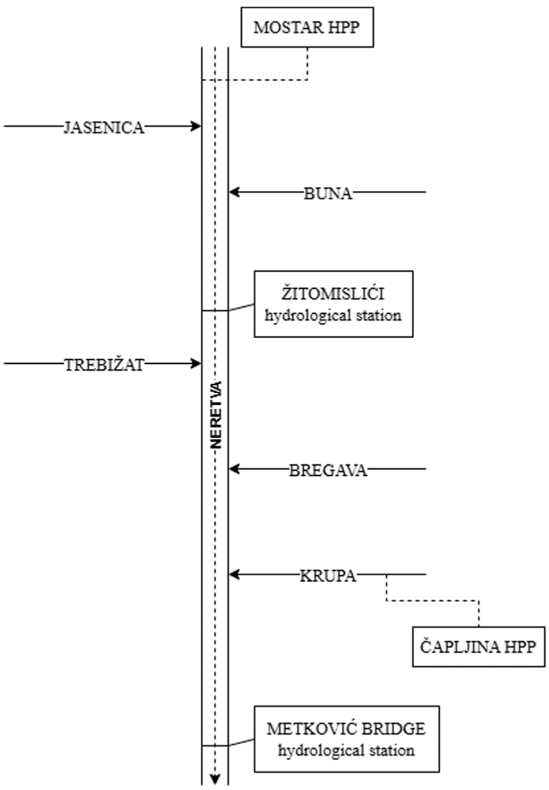

Fig. 15. Schematic overview of River Neretva hydrological stations and tributaries between HPP Mostar and Metković bridge.

Table 2
Average, minimum and maximum annual discharge values for Trebižat and Bregava.

	Trebižat ($m^3\ s^{-1}$)			Bregava ($m^3\ s^{-1}$)		
Year	**Average**	**Minimum**	**Maximum**	**Average**	**Minimum**	**Maximum**
2019	29.6	3.41	138.0	13.7	0.245	49.3
2018	25.5	1.76	110.0	15.4	0.091	50.6
2017	12.5	1.24	120.0	8.38	0.107	43.8
2016	16.1	2.94	98.7	12.9	0.365	45.2
2015	26.6	3.0	151.0	10.8	0.107	45.2
2014	39	4.5	151.0	14.7	0.73	44.9
2013	45.9	2.04	116.0	17.3	0.268	44.2

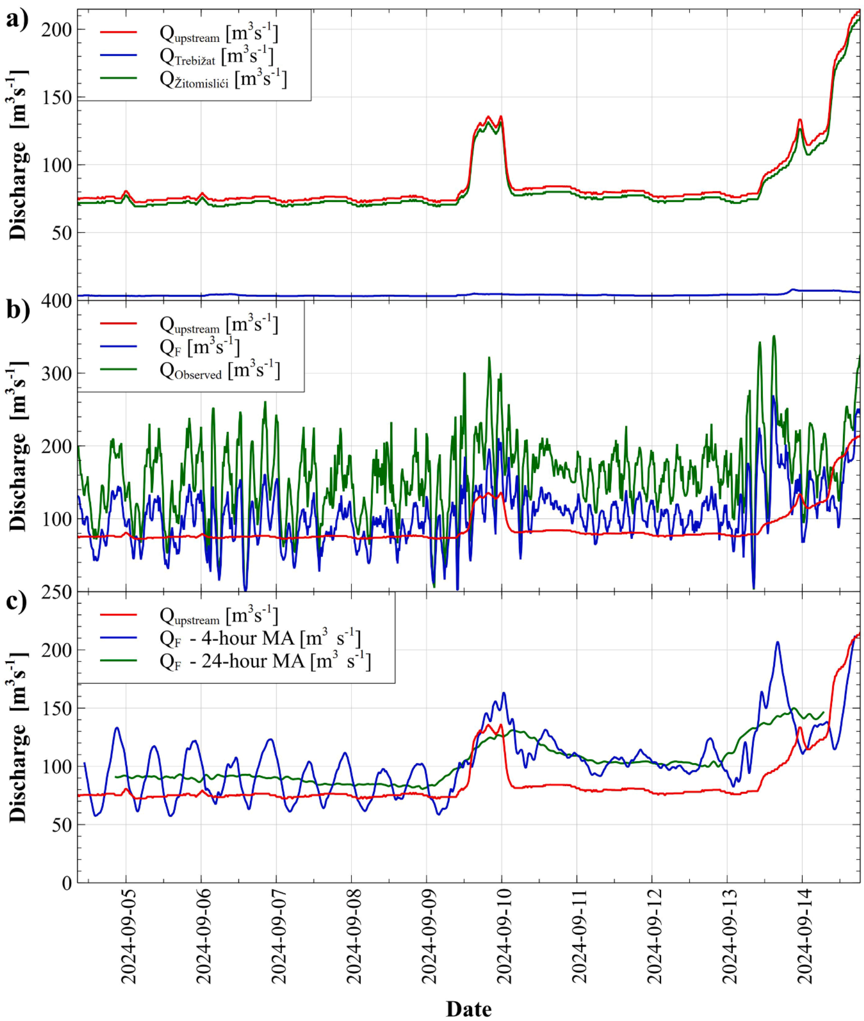

Fig. 16. a) Discharge values for Žitomislići and Trebižat hydrological station and $Q_{upstream}$; b) Discharge values of the $Q_{upstream}$, Q_F and $Q_{Observed}$ c) Discharge value of the $Q_{upstream}$, 24-hour trend for Q_F and precipitation at Ploče meteorological station.

minimal HPP regulation, Q_F 24-hour trend progressively converges towards $Q_{upstream}$ values (Fig. 16c) due to very low discharge values characterising left bank tributaries Bregava and Krupa (Table 2). Conversely, during abrupt discharge increases triggered by extensive precipitation and HPP operations, Q_F 24-hour trend temporarily falls slightly below $Q_{upstream}$. This local apparent underestimation arises from the transformation of the $Q_{upstream}$ hydrogram as the pulse travels downstream to the Metković bridge profile. Another period characterised by the precipitation absence (September 11th – September 13th) in Fig. 16c highlights enlarged difference between $Q_{upstream}$ and Q_F 24-hour trend but similar relative features with the period September 4th to September 9th 2024. The increase of the internal difference can be found in the response of the basin to previously occurred precipitation and increase of the tributaries discharge inflow along this period. As shown, differences in Q_F and $Q_{upstream}$ are justified by separate contribution of lateral inflow and HPP operation along and upstream from the Neretva estuary. Comparison performed enables qualitative validation of the Q_F with additional support of available quantitative intervals and discharge observations on site.

Relative comparison of the results obtained in this paper can be qualitatively done with the study by (Mihel et al., 2025) who implemented wide set of regression based machine learning methods to estimate freshwater discharge in tidally dominated Neretva estuary. Although the results showed great capability to capture for natural freshwater discharge during the rain season (discharge greater than app. 300 $m^3 s^{-1}$), dry season (August) results indicated discrepancies in standard deviation compared to observed Metković bridge discharge. The latter highlights physical and mass conservation fulfilment superiority of the proposed framework to assess Q_F in this paper, as well as limitations present in considering $Q_{Observed}$ values at Metković bridge as reliable during tide dominated conditions (discharge lower than app. 300 $m^3 s^{-1}$).

4.3. Freshwater discharge and observed discharge ratio

The flow in upper freshwater layer Q_F is representative of freshwater discharge during periods when the salt wedge is evident at Metković bridge profile. These periods are characterised by $Q_{Metković}$ values found below approximately 300 $m^3 s^{-1}$. As the salt wedge migrates upstream or downstream due to the interplay of Q_F and h_{SL}, the h_{SFI} rises and falls at observation profile. Upstream intrusion of the salt wedge results in minimization of h_{SFI} values, whereas salt wedge retreat leads to increase h_{SFI} values up to maximum riverbed bottom depth. When SFI diminishes from the water column profile, Q_F corresponds to $Q_{Metković}$, since the salt wedge is absent from Metković bridge profile and A_F is equal to A_0. As h_{SFI} values decreases, the difference between Q_F and $Q_{Metković}$ is more pronounced, reaching its maximum for h_{SFI} values observed at the highest elevated sensor at installed temperature chain. With freshwater discharge increase or decrease, salt wedge moves downstream or upstream resulting in h_{SFI} increase or decrease at Metković bridge profile. As the h_{SFI} difference relative to maximum river depth increases, Q_F more closely fulfils the two-layer conceptual flow model and deviate from $Q_{Metković}$ values. In case of stratification absence, the ratio between Q_F and $Q_{Metković}$ equals to unity, unless in highly stratified water column conditions the ratio takes smaller values.

4.4. Tidal influence to freshwater discharge

As shown in (Krvavica et al., 2025) the presence of tidal modulation in River Neretva surface level oscillation has been evidenced during dry period. Apart from tidal influence to Neretva water level, strong influence of the tides to stream velocities at Metković profile has been identified hereby based on the ASD and cross-correlation analysis. Match in tidal dominant constituents shown in Fig. 10 a, c and d indicates influence of h_{SL} fluctuations to stream flow velocity within the backwater zone. By taking into consideration Q_F is assessed via Eq. 6, it is straightforward the framework incorporates the backwater effect to stream velocity values. After detection of tidal constituents by ASD analysis, cross-correlation is applied to check the degree of similarity between h_{SL} and U_{middle} observed time-series as a function of the time lag. Cross-correlation analysis performed between h_{SL} and U_{middle} results in maximum cross-correlation factor (CCF) of 0.4781 for 10 time steps lag corresponding to 2.5-hour delay of the stream velocity relative to changes in h_{SL}. Observed stream velocities cannot be thus considered solely river-driven in surface layer of the salt wedge as tidal oscillations contribute to their modulation in both scalar and vector components. Proposed framework incorporates the influence of tidal dynamics on freshwater discharge determination in backwater-affected environment of the Neretva estuary via observed stream velocity values influenced by tides.

4.5. Freshwater discharge assessment procedure relevance and application

Q_F assessment procedure for stratified conditions presents improvement in River Neretva estuary discharge definition since it excludes seawater cross-sectional area and gives more realistic values of discharge value in the upper layer. The basis for Q_F assessment is the stream velocity observed by H-ADCP at Metković bridge hydrological profile as a first order data influenced by backwater effect from the Adriatic Sea, thus taking into account tidal influence. Several studies addressed challenges in estimating freshwater discharge in tidally influenced, stratified estuaries using H-ADCP measurements at bridge or cross-sectional profiles. These papers highlighted improvements like excluding seawater-influenced areas or cross-sections to yield more realistic freshwater values, taking into account backwater from the sea, sidewall effects, and stratification in salt-wedge or partially mixed estuaries.

(Sassi et al., 2011) developed a method for continuous discharge estimation in a tidally influenced river by using H-ADCP data for more accurate total flows under tidal backwater, with intratidal variations prominent only at low river discharges. Focused on backwater-affected meandering rivers, (Hidayat et al., 2011) used vertical velocity profiling and implicitly handles of upper-layer dynamics by excluding tidal and lake backwater influences for more realistic freshwater estimate.

Additional capacity to assess freshwater discharge in stratified conditions has been reported by (Moftakhari et al., 2013) whose work was founded on astronomical forcing and tidal statistics. Tidal observation were used as a in work by (Cai et al., 2014) to estimate freshwater discharge in Yangze estuary.

To end this, proposed framework of Q_F determination represents a first order data-based way to obtain freshwater discharge in highly stratified estuaries. Under the term of first order data, the knowledge of riverbed geometry, upper layer stream velocity and water surface elevation is a priori considered thus leading to three parametric framework application.

4.6. Moving average time scale selection and compliance to periodicity features

Selection of the relevant MA time scales is based on the natural periodicity found within the time series of interest of this study. Sudden increases in discharge values, observed both in the $Q_{upstream}$ and Q_F time series, can be attributed to operational releases from upstream HPPs with temporal periodicity different than tidal ones. The initial justification on relevant periodicity time scales is based on frequency patterns insight found in the ASD analysis results presented in Fig. 10. Observed time series of Q_F, h_{SL}, U_{middle} and h_{SFI} (a) showed dominant frequency peaks corresponding to long-term trends (low-frequency bands), 24-hour, 12-hour and 4-hour corresponding periodicities. Unless 12- and 24-hours frequency constituents are well known tidal induced ones, the presence of 4-hour corresponding constituents in the Q_F implies the periodic change in hydrological pattern caused by upstream HPP operations. Following the approximate identification of characteristic periods, sensitivity analyses were conducted to confirm main periodicity constituents as well as the positions and length of the time spans characterised by Q_F dominance.

24-hour MA contributes the observed h_{SFI} time series with the best trend and residual based information ($R^2 = 0.658$, CE = 0.66 and RMSE = 0.238) confirming overall presence of tidal constituents along 11 days' period of interest. The 4-hour MA contributes to the observed h_{SFI} time series along the Q_F dominated periods, with Q_F trend-based information solely contributing to h_{SFI} ($R^2 = 0.836$, CE = 0.877 and RMSE = 0.151). This identifies that the dominant periodicity in the h_{SFI} signal along the increased Q_F time spans corresponds to 4 h, which is in compliance with ASD obtained features.

Inspection of the Eqs. (18) – (20) framework sensitivity to the selection of the window lengths corresponding to discharge dominated periods has been performed on: i) Period 1 - from September 9th 2024 at 2:15 AM to September 9th 2024 and ii) Period 2 - from September 12th 2024 at 6:30 AM to September13th 2024 at 5:30 PM. Application of Eqs. (18) - (20) with the involvement of the window time spans extension/reduction leads to the fact maximum framework capacity to mimic observed h_{SFI} is obtained with $R^2 = 0.861$, CE = 0.862 and RMSE = 0.151 for the Period 1, and $R^2 = 0.861$, CE = 0.862 and RMSE = 0.151 for Period 2.

5. Conclusions

This study presents two main novelties and contributions: i) novel temperature-based monitoring approach planned, developed and implemented to the River Neretva to assess seawater-freshwater interface (SFI) dynamics in microtidal highly stratified estuaries and ii) identification of spectral constituents' correspondence of the h_{SFI} and its controlling mechanisms: tidal induces sea level oscillations and upstream freshwater discharge.

Based on the data analyses obtained by the novel monitoring approach, the main hydrological findings for the River Neretva area can be summarized as follows:

- T sensor chain enables continuous, process adjusted resolution for vertical temperature stratification observation and allows accurate delineation of the SFI depth and shape. This approach overcomes limitations of traditional EC-based monitoring by providing a cost-effective and low-maintenance alternative.
- Based on accurate h_{SFI} determination, the correction of freshwater discharge values corresponding to stratified flow conditions ensures accurate and reliable freshwater amount crucial for water management purposes. As the freshwater discharge is defined as main controlling factor controlling the salt wedge length (Geyer and Ralston, 2011), even negligible deviations from accurate value can lead to its over or underestimation during the dry season when highly stratified conditions along the estuaries are faced with. Dry periods presence in estuaries along Mediterranean can take up to 7–8 months (Lovrinović et al., 2023; Zachopoulos et al., 2020) emphasizing the demand for this improvement. Furthermore, accurate freshwater discharge presents essential input for sustainable water management in River Neretva as well as in other coastal areas ensuring the preservation of water quality and preservation of coastal biodiversity (Feng and Chen, 2023).
- SFI dynamics as demonstrated, is simultaneously controlled by upstream freshwater discharge and tidal oscillations in Neretva estuary during analysed period, each operating on different timescales. Decomposition of time series into trend and residual components highlights long-term SFI depth trend is predominantly governed by freshwater discharge trend variations which is in compliance to previous findings by Krvavica et al. (2021), unless short-term SFI oscillations corresponds to tidal forcing even in microtidal estuaries which is in agreement to Consuegra et al. (2024).
- Unless previous results on the Neretva estuary SWI showed the upstream river inflow has the strongest impact on the salt-wedge dynamics, while tidal induced sea-level reflects smaller changes in salt wedge parameters (Krvavica et al., 2021), our findings demonstrate dominant importance of the tides in the frequency pattern of the SFI depth during dry season conditions. Rate of h_{SFI} change induced by the change in the upstream freshwater discharge is shown to be + /- 0.1 m per -/ + 10 $m^3 s^{-1}$ at Metković bridge hydrological profile. Equivalent change of the h_{SFI} compared to tidal oscillations is ensured in between intratidal semi-diurnal oscillation occurrence highlighting the dominance of the tides in h_{SFI} transient nature.
- The transition from dry to rain season, either to periods with intensified operational discharge release from the HPP's upstream, highlights the dominance of freshwater discharge influence over the diminishing tidal effects in the SFI definition at the Metković bridge station.
- The establishment of a simple linear model as an assessment framework for h_{SFI} determination in highly stratified estuaries allows to identify separate either cumulative contributions of upstream freshwater discharge and downstream sea level to define h_{SFI} during 11 days' period of interest. Furthermore, based on the performed validation, the framework highlights potential applicability to other sites.

To end this, the research presented in this paper contributes to better understanding of SFI transient behaviour in River Neretva microtidal estuary with a monitoring framework to improve freshwater discharge assessment in highly stratified conditions. Based on the performed short term validation, assessment framework relying on 11 days' observation period is shown to provide a valuable and practical tool to assess h_{SFI} along the short-term period present in microtidal estuary during dry season condition, with potential for further development and improvements.

CRediT authorship contribution statement

Marin Milin: Validation, Investigation, Data curation. **Veljko Srzić:** Writing – review & editing, Validation, Supervision, Methodology, Investigation, Funding acquisition, Formal analysis, Conceptualization. **Iva Aljinović:** Writing – review & editing, Writing – original draft, Visualization, Validation, Methodology, Investigation, Formal analysis, Data curation, Conceptualization.

Funding

This research is funded by the contribution from the EU co-financing, the Interreg Croatia - Bosnia and Herzegovina - Montenegro IPA CBC Programme 2021–2027 call as a part of project Monitoring interaction between the ground and surface Water to improve the sustainable agricultural resilience to climate changes impact in coastal systems (MoWaCLIM) (HR-BA-ME00405) and the Interreg Italy - Croatia CBC Programme 2021–2027 call as a part of project Subsurface WAter monitoring and Management to prevent drought risk in coastal systems (SWAMrisk) (ITHR0200479).

Declaration of Competing Interest

The authors declare that they have no known competing financial interests or personal relationships that could have appeared to influence the work reported in this paper.

Appendix A. Supporting information

Supplementary data associated with this article can be found in the online version at doi:10.1016/j.ejrh.2026.103607.

Data availability

The authors do not have permission to share data.

References

Abramic, A., Martínez-Alzamora, N., González Del Rio Rams, J., Barrachina, T., Polo, J.F., 2014. New methodology for analysing and increasing the cost-efficiency of environmental monitoring networks. Mar. Pollut. Bull. 86, 161–173. https://doi.org/10.1016/j.marpolbul.2014.07.029.

Bonacci, O., Željković, I., Galić, A., 2013. Karst rivers' particularity: an example from Dinaric karst (Croatia/Bosnia and Herzegovina). Environ. Earth Sci. 70, 963–974. https://doi.org/10.1007/s12665-012-2187-9.

Box, G.E.P., Jenkins, G.M., Reinsel, G.C., Ljung, G.M., 2016. Time series analysis: forecasting and control, Fifth edition. ed. Wiley series in probability and statistics. Wiley, Hoboken, New Jersey.

Cai, H., Savenije, H.H.G., Jiang, C., 2014. Analytical approach for predicting fresh water discharge in an estuary based on tidal water level observations. Hydrol. Earth Syst. Sci. 18, 4153–4168. https://doi.org/10.5194/hess-18-4153-2014.

Cardona, Y., Álvarez-Silva, Ó., Barrios, Y., Saavedra, V., Cáceres-Euse, A., Cantero, M.A., Osorio, A.F., 2025. Influence of river discharge and tides on the salinity structure at the Magdalena River Estuary. Estuaries Coasts 48, 23. https://doi.org/10.1007/s12237-024-01435-7.

Chong, Y.J., Khan, A., Scheelbeek, P., Butler, A., Bowers, D., Vineis, P., 2014. Climate change and salinity in drinking water as a global problem: using remote-sensing methods to monitor surface water salinity. Int. J. Remote. Sens. 35, 1585–1599. https://doi.org/10.1080/01431161.2013.878065.

Consuegra, C., Ospino, S., Pierini, J.O., Orejarena, A., Álvarez, O.A., Toro, V.G., Restrepo, J.C., 2024. Density gradient effect on circulation patterns and mixing processes: Observations at the convergence front of a salt wedge, microtidal estuary. Reg. Stud. Mar. Sci. 75, 103569. https://doi.org/10.1016/j.rsma.2024.103569.

Cordero-Acosta, J.R., Otero Díaz, L.J., Higgins Álvarez, A.E., 2024. Influence of Fluvial Discharges and Tides on the Salt Wedge Position of a Microtidal Estuary: Magdalena River. Water 16, 1139. https://doi.org/10.3390/w16081139.

Elliott, M., Whitfield, A.K., 2011. Challenging paradigms in estuarine ecology and management. Estuar. Coast. Shelf Sci. 94, 306–314. https://doi.org/10.1016/j.ecss.2011.06.016.

Federalni hidrometeorološki zavod, 2022. Hidrološki godišnjak: Knjiga 1 – Hidrologija 2019.

Feng, X., Chen, J., 2023. Impacts of environmental factors and freshwater discharges from multiple river outlets on estuarine salinity variation in rainy season: A case study of the Pearl River Estuary in China. J. Hydrol. 623, 129784. https://doi.org/10.1016/j.jhydrol.2023.129784.

FGAG, 2023. Salinity Monitoring at Lower Neretva Area—Report for the Year.

Gaiolini, M., Colombani, N., Mastrocicco, M., Postacchini, M., 2023. Seawater intrusion assessment along the Volturno River (Italy) via numerical modeling and spectral analysis. J. Hydrol. 626, 130289. https://doi.org/10.1016/j.jhydrol.2023.130289.

Geyer, W.R., MacCready, P., 2014. The Estuarine Circulation. Annu. Rev. Fluid. Mech. 46, 175–197. https://doi.org/10.1146/annurev-fluid-010313-141302.

Geyer, W.R., Ralston, D.K., 2011. The Dynamics of Strongly Stratified Estuaries. Treatise on Estuarine and Coastal Science. Elsevier, pp. 37–51. https://doi.org/10.1016/B978-0-12-374711-2.00206-0.

Hansen, D.V., Rattray, M., 1966. New dimensions in estuary classification1. Limnol. & Oceanogr. 11, 319–326. https://doi.org/10.4319/lo.1966.11.3.0319.

Hansun, S., 2013. A new approach of moving average method in time series analysis. 2013 Conference on New Media Studies (CoNMedia). Presented at the 2013 Conference on New Media Studies (CoNMedia). IEEE, Tangerang, Indonesia, pp. 1–4. https://doi.org/10.1109/CoNMedia.2013.6708545.

Haralambidou, K., Sylaios, G., Tsihrintzis, V.A., 2010. Salt-wedge propagation in a Mediterranean micro-tidal river mouth. Estuar. Coast. Shelf Sci. 90, 174–184. https://doi.org/10.1016/j.ecss.2010.08.010.

Hayashi, M., 2004. Temperature-electrical conductivity relation of water for environmental monitoring and geophysical data inversion. Environ. Monit. Assess. 96, 119–128. https://doi.org/10.1023/B:EMAS.0000031719.83065.68.

He, W., Zhang, J., Yu, X., Chen, S., Luo, J., 2018. Effect of runoff variability and sea level on saltwater intrusion: a case study of Nandu River Estuary, China. Water Resour. Res. 54, 9919–9934. https://doi.org/10.1029/2018WR023285.

Hidayat, H., Vermeulen, B., Sassi, M.G., Torfs, P.J.J.F., Hoitink, A.J.F., 2011. Discharge estimation in a backwater affected meandering river. Hydrol. Earth Syst. Sci. 15, 2717–2728. https://doi.org/10.5194/hess-15-2717-2011.

Hidayat, H., Hoitink, A.J.F., Sassi, M.G., Torfs, P.J.J.F., 2014. Prediction of discharge in a tidal river using artificial neural networks. J. Hydrol. Eng. 19, 04014006. https://doi.org/10.1061/(ASCE)HE.1943-5584.0000970.

Higgins Álvarez, A., Otero, L., Restrepo, J.C., Álvarez, O., 2022. The effect of waves in hydrodynamics, stratification, and salt wedge intrusion in a microtidal estuary. Front. Mar. Sci. 9, 974163. https://doi.org/10.3389/fmars.2022.974163.

Janeković, I., Kuzmić, M., 2005. Numerical simulation of the Adriatic Sea principal tidal constituents. Ann. Geophys. 23, 3207–3218. https://doi.org/10.5194/angeo-23-3207-2005.

Jeon, W., Moon, H.S., Choi, J., Jung, B., Kim, Y., Hwang, S., Lee, S., 2024. An Automatic-Vertical Profile Monitoring System for Fresh–Saline Water Zones in Coastal Aquifer. Groundwater 62, 635–644. https://doi.org/10.1111/gwat.13366.

Jiang, D., Dong, C., Ma, Z., Wang, X., Lin, K., Yang, F., Chen, X., 2024. Monitoring saltwater intrusion to estuaries based on UAV and satellite imagery with machine learning models. Remote. Sens. Environ. 308, 114198. https://doi.org/10.1016/j.rse.2024.114198.

Kennish, M.J., 2002. Environmental threats and environmental future of estuaries. Envir. Conserv. 29, 78–107. https://doi.org/10.1017/S0376892902000061.

Khojasteh, D., Chen, S., Felder, S., Heimhuber, V., Glamore, W., 2021. Estuarine tidal range dynamics under rising sea levels. PLoS. ONE 16, e0257538. https://doi.org/10.1371/journal.pone.0257538.

Kostaschuk, R.A., Atwood, L.A., 1990. River discharge and tidal controls on salt-wedge position and implications for channel shoaling: Fraser River, British Columbia. Can. J. Civ. Eng. 17, 452–459. https://doi.org/10.1139/l90-049.

Krishna, H., 2017. Digital Signal Processing Algorithms (ed). Number Theory, Convolution, Fast Fourier Transforms, and Applications, First edition. Taylor and Francis, London.

Krvavica, N., Ružić, I., 2020. Assessment of sea-level rise impacts on salt-wedge intrusion in idealized and Neretva River Estuary. Estuar. Coast. Shelf Sci. 234, 106638. https://doi.org/10.1016/j.ecss.2020.106638.

Krvavica, N., Gotovac, H., Lončar, G., 2021. Salt-wedge dynamics in microtidal Neretva River estuary. Reg. Stud. Mar. Sci. 43, 101713. https://doi.org/10.1016/j.rsma.2021.101713.

Krvavica, N., Gržić, M.M., Innocenti, S., Matte, P., 2025. Impact of storm surge and power peaking on tidal-fluvial processes in microtidal Neretva River estuary. Estuar. Coast. Shelf Sci. 318, 109227. https://doi.org/10.1016/j.ecss.2025.109227.

Lee, M., Yoo, Y., Joo, H., Kim, K.T., Kim, H.S., Kim, S., 2021. Construction of rating curve at high water level considering rainfall effect in a tidal river. J. Hydrol. Reg. Stud. 37, 100907. https://doi.org/10.1016/j.ejrh.2021.100907.

Li, L., Zhu, J., Chant, R.J., Wang, C., Pareja-Roman, L.F., 2020. Effect of Dikes on Saltwater Intrusion Under Various Wind Conditions in the Changjiang Estuary. JGR Oceans 125, e2019JC015685. https://doi.org/10.1029/2019JC015685.

Ljubenkov, I., Vranješ, M., 2012. Numerical model of stratified flow – case study of the Neretva riverbed salination (2004). JCE 64, 101–113. https://doi.org/10.14256/JCE.639.2011.

Lovrinović, I., Bergamasco, A., Srzić, V., Cavallina, C., Holjević, D., Donnici, S., Erceg, J., Zaggia, L., Tosi, L., 2021. Groundwater Monitoring Systems to Understand Sea Water Intrusion Dynamics in the Mediterranean: The Neretva Valley and the Southern Venice Coastal Aquifers Case Studies. Water 13, 561. https://doi.org/10.3390/w13040561.

Lovrinović, I., Srzić, V., Aljinović, I., 2023. Characterization of seawater intrusion dynamics under the influence of hydro-meteorological conditions, tidal oscillations and melioration system operative regimes to groundwater in Neretva valley coastal aquifer system. J. Hydrol. Reg. Stud. 46, 101363. https://doi.org/10.1016/j.ejrh.2023.101363.

MacCready, P., Geyer, W.R., 2010. Advances in Estuarine Physics. Annu. Rev. Mar. Sci. 2, 35–58. https://doi.org/10.1146/annurev-marine-120308-081015.

Mazhar, S., Pellegrini, E., Contin, M., Bravo, C., De Nobili, M., 2022. Impacts of salinization caused by sea level rise on the biological processes of coastal soils - A review. Front. Environ. Sci. 10, 909415. https://doi.org/10.3389/fenvs.2022.909415.

McKeon, M.A., Horner-Devine, A.R., Giddings, S.N., 2021. Seasonal Changes in Structure and Dynamics in an Urbanized Salt Wedge Estuary. Estuaries Coasts 44, 589–607. https://doi.org/10.1007/s12237-020-00788-z.

Mihel, A.M., Krvavica, N., Lerga, J., 2025. Regression-based machine learning approaches for estimating discharge from water levels in microtidal rivers. J. Hydrol. 646, 132276. https://doi.org/10.1016/j.jhydrol.2024.132276.

Moftakhari, H.R., Jay, D.A., Talke, S.A., Kukulka, T., Bromirski, P.D., 2013. A novel approach to flow estimation in tidal rivers. Water Resour. Res. 49, 4817–4832. https://doi.org/10.1002/wrcr.20363.

Montgomery, D.C., Peck, E.A., Vining, G.G., 2021. Introduction to linear regression analysis. Wiley series in probability and statistics, Sixth edition. Wiley, Hoboken, New Jersey.

Nguyen, D.H., Umeyama, M., Shintani, T., 2012. Importance of geometric characteristics for salinity distribution in convergent estuaries. J. Hydrol. 448449 1–13. https://doi.org/10.1016/j.jhydrol.2011.10.044.

Otero, L.J., Hernandez, H.I., Higgins, A.E., Restrepo, J.C., Álvarez, O.A., 2021. Interannual and seasonal variability of stratification and mixing in a high-discharge micro-tidal delta: Magdalena River. J. Mar. Syst. 224, 103621. https://doi.org/10.1016/j.jmarsys.2021.103621.

Perales-Valdivia, H., Sanay-González, R., Valle-Levinson, A., 2018. Effects of tides, wind and river discharge on the salt intrusion in a microtidal tropical estuary. Reg. Stud. Mar. Sci. 24, 400–410. https://doi.org/10.1016/j.rsma.2018.10.001.

Poggioli, A.R., Horner-Devine, A.R., 2015. The Sensitivity of Salt Wedge Estuaries to Channel Geometry. J. Phys. Oceanogr. 45, 3169–3183. https://doi.org/10.1175/JPO-D-14-0218.1.

Postacchini, M., Manning, A.J., Calantoni, J., Smith, J.P., Brocchini, M., 2023. A storm driven turbidity maximum in a microtidal estuary. Estuar. Coast. Shelf Sci. 288, 108350. https://doi.org/10.1016/j.ecss.2023.108350.

Pritchard, D.W., 1955. Estuarine Circulation Patterns. Proc. Am. Soc. Civil. Eng. 81, 1–11.

Racetin, I., Krtalic, A., Srzic, V., Zovko, M., 2020. Characterization of short-term salinity fluctuations in the Neretva River Delta situated in the southern Adriatic Croatia using Landsat-5 TM. Ecol. Indic. 110, 105924. https://doi.org/10.1016/j.ecolind.2019.105924.

Reed, R.E., Glasgow, H.B., Burkholder, J.M., Brownie, C., 2004. Seasonal physical–chemical structure and acoustic Doppler current profiler flow patterns over multiple years in a shallow, stratified estuary, with implications for lateral variability. Estuar. Coast. Shelf Sci. 60, 549–566. https://doi.org/10.1016/j.ecss.2004.02.010.

Rummel, K., Strauß, T., Lauer, F., Gräwe, U., 2025. Real-Time Prediction of Salt Intrusion in Tidal Estuaries Using Long Short-Term Memory Networks. J. Geophys. Res. Mach. Learn. Comput. 2, e2025JH000768. https://doi.org/10.1029/2025JH000768.

Sassi, M.G., Hoitink, A.J.F., Vermeulen, B., Hidayat, 2011. Discharge estimation from H-ADCP measurements in a tidal river subject to sidewall effects and a mobile bed. Water Resour. Res. 47, 2010WR009972. https://doi.org/10.1029/2010WR009972.

Savenije, H.H.G., 2005. Salinity and Tides in Alluvial Estuaries. Elsevier. https://doi.org/10.1016/B978-0-444-52107-1.X5000-X.

Setiawan, I., Morgan, L.K., Doscher, C., 2023. Saltwater intrusion from an estuarine river: A field investigation. J. Hydrol. 617, 128955. https://doi.org/10.1016/j.jhydrol.2022.128955.

Srzić, V., Lovrinović, I., Racetin, I., Pletikosić, F., 2020. Hydrogeological characterization of coastal aquifer on the basis of observed sea level and groundwater level fluctuations: neretva valley aquifer, Croatia. Water 12, 348. https://doi.org/10.3390/w12020348.

Thomson, R.E., Emery, W.J., 2014. Time Series Analysis Methods. Data Analysis Methods in Physical Oceanography. Elsevier, pp. 425–591. https://doi.org/10.1016/B978-0-12-387782-6.00005-3.

Tosi, L., Cosma, M., Yaciuk, P.A., Aljinović, I., Artuso, A., Čarija, J., Da Lio, C., Frison, L., Srzić, V., Tateo, F., Donnici, S., 2025. Developing integrated supersites to advance the understanding of saltwater intrusion in the coastal plain between the Brenta and Adige Rivers, Italy. JMSE 13, 2328. https://doi.org/10.3390/jmse13122328.

Vallejos, A., Sola, F., Pulido-Bosch, A., 2015. Processes Influencing Groundwater Level and the Freshwater-Saltwater Interface in a Coastal Aquifer. Water Resour. Manag. 29, 679–697. https://doi.org/10.1007/s11269-014-0621-3.

Wegman, T.M., Pietrzak, J.D., Horner-Devine, A.R., Dijkstra, H.A., Ralston, D.K., 2025. Observations of Estuarine Salt Intrusion Dynamics During a Prolonged Drought Event in the Rhine-Meuse Delta. JGR Oceans 130, e2024JC021655. https://doi.org/10.1029/2024JC021655.

Werner, A.D., Bakker, M., Post, V.E.A., Vandenbohede, A., Lu, C., Ataie-Ashtiani, B., Simmons, C.T., Barry, D.A., 2013. Seawater intrusion processes, investigation and management: Recent advances and future challenges. Adv. Water Resour. 51, 3–26. https://doi.org/10.1016/j.advwatres.2012.03.004.

Wullems, B.J.M., Brauer, C.C., Baart, F., Weerts, A.H., 2023. Forecasting estuarine salt intrusion in the Rhine–Meuse delta using an LSTM model. Hydrol. Earth Syst. Sci. 27, 3823–3850. https://doi.org/10.5194/hess-27-3823-2023.

Zachopoulos, K., Kokkos, N., Sylaios, G., 2020. Salt wedge intrusion modeling along the lower reaches of a Mediterranean river. Reg. Stud. Mar. Sci. 39, 101467. https://doi.org/10.1016/j.rsma.2020.101467.

Zhang, Z., Savenije, H.H.G., 2018. Thermodynamics of saline and fresh water mixing in estuaries. Earth Syst. Dynam 9, 241–247. https://doi.org/10.5194/esd-9-241-2018.